

Luminosity distance in Swiss cheese cosmology with randomized voids. II. Magnification probability distributions

Éanna É. Flanagan,^{1,2,*} Naresh Kumar,^{1,†} Ira Wasserman,^{1,2,‡} and R. Ali Vanderveld^{3,§}

¹Laboratory for Elementary Particle Physics, Cornell University, Ithaca, NY 14853, USA

²Center for Radiophysics and Space Research, Cornell University, Ithaca, NY 14853, USA

³Kavli Institute for Cosmological Physics, University of Chicago, Chicago, Illinois 60637, USA

We study the fluctuations in luminosity distances due to gravitational lensing by large scale ($\gtrsim 35$ Mpc) structures, specifically voids and sheets. We use a simplified “Swiss cheese” model consisting of a Λ CDM Friedman-Robertson-Walker background in which a number of randomly distributed non-overlapping spherical regions are replaced by mass compensating comoving voids, each with a uniform density interior and a thin shell of matter on the surface. We compute the distribution of magnitude shifts using a variant of the method of Holz & Wald (1998), which includes the effect of lensing shear. The standard deviation of this distribution is ~ 0.027 magnitudes and the mean is ~ 0.003 magnitudes for voids of radius 35 Mpc, sources at redshift $z_s = 1.0$, with the voids chosen so that 90% of the mass is on the shell today. The standard deviation varies from 0.005 to 0.06 magnitudes as we vary the void size, source redshift, and fraction of mass on the shells today. If the shell walls are given a finite thickness of ~ 1 Mpc, the standard deviation is reduced to ~ 0.013 magnitudes. This standard deviation due to voids is a factor ~ 3 smaller than that due to galaxy scale structures. We summarize our results in terms of a fitting formula that is accurate to $\sim 20\%$, and also build a simplified analytic model that reproduces our results to within $\sim 30\%$. Our model also allows us to explore the domain of validity of weak lensing theory for voids. We find that for 35 Mpc voids, corrections to the dispersion due to lens-lens coupling are of order $\sim 4\%$, and corrections to due shear are $\sim 3\%$. Finally, we estimate the bias due to source-lens clustering in our model to be negligible.

I. INTRODUCTION

A. Background and Motivation

A number of surveys are being planned to determine luminosity distances to various different astronomical sources, and to use them to constrain properties of the dark energy or modifications to gravity that drive the cosmic acceleration. It has long been recognized that perturbations to luminosity distances from weak gravitational lensing will be a source of error for these studies, both statistical and systematic [1–5]. For supernovae the lensing noise becomes significant only at high redshifts [6], but for gravitational wave sources the lensing noise dominates over the intrinsic luminosity scatter [7, 8]. Theoretical predictions for the magnification probability distribution can be folded into the data analysis of surveys to improve the results [9], and in particular it is possible to exploit the known non-Gaussian nature of this distribution [10]. In addition, it is possible to treat the “lensing noise” in luminosity distances as a signal in its own right, which provides useful information [11]. (A tentative detection of this signal in supernovae data has been claimed in Ref. [12].) For these reasons, it is useful to have a detailed understanding of the magnification

probability distribution.

There are a number of methods that have been used to study the effects of weak lensing on luminosity distances:

- Weak lensing theory can be used to predict the variance of the magnification distribution from the matter power spectrum [13]. However, the accuracy of this approach is limited and in particular it does not allow one to probe the non-Gaussian tails of the distribution¹.
- One can use numerical ray tracing using the results of cosmological simulations of large scale structure, such as the Millennium simulation [15] and the Coyote Universe project [16], see, eg. Ref. [17]. This approach is highly accurate and is based on a realistic density distribution. However it requires substantial computational power and is also limited in some other respects. The largest simulations to date are confined to a cube of comoving size $z \sim 0.16$, so only a limited range of source redshifts can be considered. Although the calculations evolve large scale structure nonlinearly, it is impractical to get a continuous description of the evolution, which is needed for computing the perturbations to light ray paths; only snapshots of the

*Electronic address: flanagan@astro.cornell.edu

†Electronic address: nk236@cornell.edu

‡Electronic address: ira@astro.cornell.edu

§Electronic address: rav@kicp.uchicago.edu

¹ We note however that there is a proposal for an approximate “universal probability distribution” for magnifications that takes as input only the variance of the distribution as predicted by weak lensing theory, and which would allow prediction of the non-Gaussian tails [14].

density distribution are available. Finally, because the calculations required to evolve the matter distribution are formidable, it can be difficult to comprehensively survey the space of the underlying parameters of the model, such as the primordial perturbation spectrum.

- A third approach is to use simplified analytical models of the distribution of matter that allow rapid computation of the full probability distribution of magnifications, see, eg., Refs. [2, 4, 18, 19].

In this paper we follow the third approach. We develop an idealized “Swiss cheese” model [2, 20–23] of large scale structure to study the effect of density inhomogeneities on luminosity distances. Our model is complementary to many of the existing models in that we focus on lensing produced by structures at the largest scales, voids and sheets, rather than that produced by individual galaxies and halos, the focus of many existing models.

B. Our void model

In “Swiss cheese” models [2, 20–23], the Universe contains a network of spherical, non-overlapping, mass-compensated voids. The voids are chosen to be mass compensated so that the potential perturbation vanishes outside each void. We idealize these models even further by assuming that each void consists of a central, uniformly underdense region surrounded by a zero thickness shell. Mass flows outward from the evacuated interior and is then trapped on the wall. Although it would be more realistic to consider voids with smooth density profiles, this very simplified model should capture the essence of the effect of large scale density inhomogeneities on luminosity distances. Since voids in the observable Universe tend to be surrounded by shells that are relatively thin compared to the size of their evacuated interiors, the idealization of zero thickness may not be a severe simplification, particularly because we expect that the main effect of inhomogeneities on the luminosity distance depends only on the integral of the density contrast along the line of sight from the source to the observer. A key feature of our idealized models is that they can be evolved in time continuously and very simply.

Within the context of this highly idealized class of models, we study the distribution of magnitude shifts relative to what would be found in a smooth cold dark matter (CDM) model of the Universe with a cosmological constant, Λ , for different void sizes and present day interior underdensities, and for a range of different source redshifts. Moreover, although we shall use a Newtonian description that is valid as long as the void radii are small enough compared with the Hubble length H_0^{-1} , the calculations can be made fully relativistic if desired. (We discuss some corrections that are higher order in $H_0 R$, where R is the void radius.)

This paper is a follow-up to our earlier work [20] (henceforth VFW08), in which we considered the effect of a randomized set of voids with a single and rather large comoving radius, 350 Mpc, using a particular model for a smooth underdense interior inside a mass compensated shell. That study found that for a source with redshift $z_s = 1.8$, the mean magnitude shift relative to smooth flat, CDM for an ensemble of realizations of large scale voids was unimportant (-0.003), but the distribution of magnitude shifts was fairly broad, with a standard deviation of about 0.1. Here, we consider a wider range of redshifts and void sizes, and compute magnitude shifts relative to a more realistic Λ CDM background with matter density today $\Omega_M = 0.3$ and dark energy density today $\Omega_\Lambda = 0.7$.

C. Predictions for lensing noise

Our results for the standard deviation σ_m of the magnitude shifts are summarized by the approximate fitting formula

$$\sigma_m \approx (0.027 \pm 0.0007) \left(\frac{R}{35 \text{ Mpc}} \right)^\alpha \left(\frac{f_0}{0.9} \right)^\beta \left(\frac{z_s}{1.0} \right)^\gamma. \quad (1.1)$$

Here R is the comoving radius of the voids, z_s is the source redshift, and f_0 is the fraction of the total void mass in its shell today. The exponents are $\alpha = 0.51 \pm 0.03$, $\beta = 1.07 \pm 0.04$, $\gamma = 1.34 \pm 0.05$. This fit is accurate to $\sim 20\%$ for $35 \text{ Mpc} \leq R \leq 350 \text{ Mpc}$, $0.01 \leq f_0 \leq 0.9$, and $0.5 \leq z_s \leq 2.1$. The mean magnitude shift is again unimportant, roughly a factor of ten smaller than the standard deviation (1.1).

Our result (1.1) is computed in the limit of zero shell thickness. This idealization is not very realistic, since as we discuss in Sec. III below there is a logarithmic divergence in the variance of the lensing convergence in the zero thickness limit. This divergence arises from rays that pass very near to the void walls. The variance in the magnitude shift, however, is finite because of the nonlinear dependence of magnitude shift on lensing convergence; the divergence is cut off at lensing convergences of order unity. (The divergence can also get regulated by finite sampling effects; see Sec. III). To address this issue we also consider a more realistic model with void walls of some finite thickness Δr . We estimate in Sec. IIID that for $f_0 = 0.9$, $R = 35 \text{ Mpc}$, and $z_s = 1.0$, the standard deviation in magnitude shift is

$$\sigma_m \approx 0.013 \sqrt{1 + 0.23 \ln \left(\frac{1 \text{ Mpc}}{\Delta r} \right)}, \quad (1.2)$$

a factor of ~ 2 smaller than the thin-shell limit (1.1) for $\Delta r = 1 \text{ Mpc}$.

The rms magnitude shift (1.2) due to voids is a factor of ~ 3 smaller than that computed from individual galaxies and halos [4], in accord with expectations from

weak lensing theory using the power spectrum of density perturbations (see Ref. [5] and Appendix A). Thus lensing due to voids is subdominant but not negligible.

We also use our model to estimate the sizes of various nonlinear effects that go beyond linear, weak-lensing theory. We estimate that for $R = 35$ Mpc voids, the dispersion σ_m is altered by $\sim 4\%$ by lens-lens coupling, by $\sim 3\%$ by shear. There are also large nonlinearities ($\sim 30\% - 40\%$) in our model that arise from the nonlinearity of void evolution. These results are qualitatively in agreement with some previous studies of nonlinear deviations from weak lensing theory [24–26].

We also study the source-lens clustering effect [27], the fact sources are more likely to be located in high density regions, which enhances the probability of a lens being located near the source. We estimate that the corresponding bias in the distribution of magnifications is negligible in our model.

D. Organization of this paper

This paper is organized as follows. Section II reviews our Swiss cheese void model. We discuss how the voids evolve in an FRW background and describe the model parameters. Next, we describe how our void locations are randomized, by choosing impact parameters randomly as light rays exit one void and enter the next. Finally, we describe our method of computing the magnification. Section III describes our simple analytical model which reproduces the results of the simulations to within $\sim 30\%$. It also describes a modification of our void model in which the shell walls are given a finite thickness, and gives the corresponding analytical results. Section IV gives the results of our Monte Carlo simulations for the probability distributions of magnifications, and discusses the dependence of the variance on the parameters of the model. In Section V, we study the source-lens clustering effect and the associated bias. Section VI summarizes our results and their implications. In Appendix A we discuss the power spectrum of our void model and the corresponding weak lensing prediction. Appendix B reviews the derivation of the method we use to compute the magnification distribution. Finally, Appendix C is a comparison of our results with other recent studies of lensing due to voids [18, 19, 28–31]. Our results are broadly consistent with these previous studies but our model is simpler in several respects.

II. SIMPLE MODEL OF LENSING DUE TO VOIDS

In this section we describe our simplified Swiss cheese model of large scale voids, and explain how we compute the distribution of magnifications in the model.

A. Newtonian model of a single void

As discussed in the introduction, we will consider void radii R ranging from 35 Mpc to 350 Mpc, which are small compared to the Hubble length. Therefore we can use Newtonian gravity to describe each void; the corresponding error is of order $(H_0 R)^2 \ll 1$ which we ignore.

We choose the background cosmology in which we place our voids to be an FRW Universe with matter fraction Ω_M and cosmological constant fraction $1 - \Omega_M$. We denote by $a_{\text{ex}}(t)$ the corresponding scale factor, which is normalized so that $a_{\text{ex}}(t) = 1$ today. It satisfies the Friedman equation

$$\left(\frac{\dot{a}_{\text{ex}}}{a_{\text{ex}}}\right)^2 = H_0^2 \left(\frac{\Omega_M}{a_{\text{ex}}^3} + 1 - \Omega_M\right), \quad (2.1)$$

where H_0 is the Hubble parameter, which has the solution

$$\frac{3H_0 t \sqrt{1 - \Omega_M}}{2} = \sinh^{-1} \left(\frac{a_{\text{ex}}^{3/2}}{a_\Lambda^{3/2}} \right). \quad (2.2)$$

Here $a_\Lambda = (\Omega_M / (1 - \Omega_M))^{1/3}$ is the scale factor at which the cosmological constant starts to dominate.

Our void model consists of a spherical region of constant comoving radius R , with a uniform density interior surrounded by a thin shell. We assume that the void is mass compensated, so the total mass enclosed is the same as what it would be in FRW, namely

$$M = \frac{H_0^2 \Omega_M R^3}{2G}. \quad (2.3)$$

We denote by $f(t)$ the fraction of this mass in the thin shell, so that the mass in the interior is $[1 - f(t)]M$. The fractional density perturbation in comoving coordinates $\delta_m(\mathbf{x}, t) = \delta\rho(\mathbf{x}, t)/\rho$ is therefore

$$\delta_m(\mathbf{x}, t) = -f(t)\Theta(R - r) + \frac{1}{3}f(t)R\delta(r - R), \quad (2.4)$$

where $\Theta(x)$ is the function defined by $\Theta(x) = 1$ for $x > 0$ and $\Theta(x) = 0$ for $x < 0$.

The corresponding potential perturbation ϕ , in a Newtonian gauge in which the metric has the form

$$ds^2 = -(1 + 2\phi) dt^2 + a_{\text{ex}}^2(t) (1 - 2\phi) d\mathbf{x}^2, \quad (2.5)$$

is given by solving the Poisson equation $\nabla^2 \phi = 3H_0^2 \Omega_M \delta_m(\mathbf{x}, t) / (2a_{\text{ex}})$. This gives

$$\phi(\mathbf{x}, t) = \frac{H_0^2 \Omega_M f(t)}{4a_{\text{ex}}(t)} (R^2 - r^2) \Theta(R - r). \quad (2.6)$$

The corresponding radial acceleration is

$$a_r = -\frac{H_0^2 \Omega_M f(t)}{2a_{\text{ex}}(t)^2} r \Theta(R - r).$$

For each void, the potential will take the form (2.6) in a spherical polar coordinate system centered on that void, and the total potential is given by summing over the voids. The potential vanishes in between the voids.

We next discuss how to compute the time evolution of the fraction $f(t)$ of the void mass in the thin shell. We will work to leading, Newtonian order in $(H_0 R)^2$, and we will also neglect the surface pressure that would arise in a relativistic calculation. The uniform interior behaves like a positive energy FRW cosmology. It has negative curvature, $k < 0$, and a scale factor $a_{\text{in}}(t)$ that obeys the equation

$$\left(\frac{\dot{a}_{\text{in}}}{a_{\text{in}}}\right)^2 = H_0^2 \left(\frac{\Omega_M}{a_{\text{in}}^3} + 1 - \Omega_M - \frac{k}{a_{\text{in}}^2 H_0^2} \right), \quad (2.7)$$

since the cosmological constant is the same inside and outside the void but the matter density is not. We define the positive constant $a_0 = -\Omega_M H_0^2 / k$, the inverse of which is proportional to the density contrast at early times. The solution to Eq. (2.7) is

$$\frac{3H_0 t \sqrt{1 - \Omega_M}}{2} = \int_0^{\left(\frac{a_{\text{in}}}{a_\Lambda}\right)^{\frac{3}{2}}} \frac{dx}{\sqrt{1 + x^2 + x^{\frac{2}{3}} \frac{a_\Lambda}{a_0}}}. \quad (2.8)$$

This solution assumes that $a_{\text{in}} = a_{\text{ex}} = 0$ at $t = 0$, so that the interior and the exterior regions started expanding at the same time. Otherwise the deviations from FRW are large at early times. Eliminating t between Eqs. (2.2) and (2.8) gives the relationship between a_{in} and a_{ex} , which is

$$\sinh^{-1} \left(\frac{a_{\text{ex}}^{3/2}}{a_\Lambda^{3/2}} \right) = \int_0^{\left(\frac{a_{\text{in}}}{a_\Lambda}\right)^{\frac{3}{2}}} \frac{dx}{\sqrt{1 + x^2 + x^{\frac{2}{3}} \frac{a_\Lambda}{a_0}}}. \quad (2.9)$$

Note that the above equations imply that $a_{\text{in}} > a_{\text{ex}}$, as $k < 0$. The density of the interior is equal to the mean FRW density times $(a_{\text{ex}}/a_{\text{in}})^3 < 1$, and so the fraction of mass in the shell is

$$f(t) = 1 - \left(\frac{a_{\text{ex}}}{a_{\text{in}}} \right)^3. \quad (2.10)$$

We numerically solve Eq. (2.9) to obtain $a_{\text{ex}}/a_{\text{in}}$ as a function of a_{ex}/a_Λ , Ω_M and a_0 . In the remainder of the paper, we will parameterize our void models in terms of the value today $f_0 = f(t_0)$ of the mass fraction $f(t)$ in the shell. We will usually pick $f_0 = 0.9$. The parameter a_0 can be computed from f_0 and Ω_M .

B. Algorithm for randomization of void placement

We now discuss how we choose the number and locations of voids in our model. In some previous studies [32–34], the centers of all the voids encountered by a given ray were chosen to be collinear, so that the ray passed through the centers of all the voids. In these studies the

lensing demagnification was large enough to successfully mimic the effects of dark energy. However, as discussed in VFW08, the large demagnification was an artifact of the non-randomness of the void locations, which is not in accord with observations of the distribution of voids [35–38]. In this paper, we use a more realistic void distribution, which we compute according to the following procedure:

1. Fix the comoving void size R .
2. Fix the redshift of the source z_s .
3. Place voids all along the ray from the source to the observer, lined up so that they are just touching. The source and the observer are placed in FRW regions. The distance from the source to the shell of the adjacent void is chosen to be a fixed small parameter, and the distance between the observer and the shell of the adjacent void then depends on the number of voids that can fit between the source and observer.
4. Randomize impact parameters by shifting each void in a random direction perpendicular to the direction of the light ray, so that the square b^2 of the impact parameter is uniformly distributed between 0 and R^2 .

Note that with this algorithm, each ray spends some time in FRW regions between each pair of voids. An alternative procedure would that used by Holz & Wald [2], in which after exiting a void, a ray immediately enters another void without traversing an FRW region. In this model the effective packing fraction of voids would be a factor ~ 2 or so higher than in our model, and the rms magnifications and demagnification would be correspondingly enhanced.

C. Method of computing magnification along a ray

We now turn to a description of the method we use to compute the magnification for a ray propagating through a Universe filled with randomly placed voids, as described in the last subsection. Our method is essentially a modification of the method introduced by Holz & Wald [2], and goes beyond weak-lensing theory. In this section we describe the computational procedure; a derivation is given in Appendix B.

Starting from the perturbed FRW metric (2.5), we consider an observer at $t = t_0$ (today) and $\mathbf{x} = 0$, or equivalently at $\eta = \eta_0$, where $\eta = \int dt/a_{\text{ex}}(t)$ is conformal time. We consider a source at $\mathbf{x} = \mathbf{x}_s = x_s \mathbf{n}$, where \mathbf{n} is a unit vector. The geodesic joining the source and observer in the background FRW geometry is

$$x^\alpha(x) = (\eta_0 - x, \mathbf{n}x), \quad (2.11)$$

for $0 \leq x \leq x_s$, where x is the comoving distance (or affine parameter with respect to the flat metric $d\bar{s}^2 =$

$a_{\text{ex}}(t)^{-2} ds^2 = -d\eta^2 + d\mathbf{x}^2$). We denote by $\vec{k} = d/dx = -\partial_\eta + n^i \partial_i$ the past directed tangent vector to the ray. We also introduce a pair of spatial basis vectors \vec{e}_A , $A = 1, 2$, so that \vec{e}_A and \mathbf{n} are orthonormal with respect to $d\bar{s}^2$. We define the projected Riemann tensor

$$\mathcal{R}_{AB} = \bar{R}_{\alpha\gamma\beta\delta} k^\gamma k^\delta e_A^\alpha e_B^\beta, \quad (2.12)$$

for $A, B = 1, 2$ where $\bar{R}_{\alpha\gamma\beta\delta}$ is the Riemann tensor of the perturbed FRW metric without the $a_{\text{ex}}(t)^2$ factor:

$$ds^2 = -(1 + 2\phi) d\eta^2 + (1 - 2\phi) d\mathbf{x}^2. \quad (2.13)$$

Next we consider the differential equation along the ray

$$\frac{d^2}{dx^2} \mathcal{A}_B^A(x) = -\mathcal{R}_C^A(x) \mathcal{A}_B^C(x), \quad (2.14)$$

where $\mathcal{R}_C^A(x)$ means the projected Riemann tensor evaluated at $x^\alpha = x^\alpha(x)$, and capital Roman indices are raised and lowered with δ_{AB} . We solve the differential equation (2.14) subject to the initial conditions at the observer

$$\mathcal{A}_B^A(0) = 0, \quad \frac{d\mathcal{A}_B^A}{dx}(0) = \delta_B^A. \quad (2.15)$$

Finally the magnification along the ray, relative to the background FRW metric, is²

$$\mu = \frac{x_s^2}{|\det \mathcal{A}(x_s)|}, \quad (2.16)$$

where the right hand side is evaluated at the location $x = x_s$ of the source.

The matrix $\mathcal{A}(x_s)/x_s$ can be expressed as a product of an orthogonal matrix and a symmetric matrix with two real eigenvalues $1 - \kappa \pm \gamma$, where κ is called the lensing convergence and γ the shear. The magnification is therefore

$$\mu = |(1 - \kappa)^2 - \gamma^2|^{-1}. \quad (2.17)$$

This computational procedure is essentially the same as that used by Holz & Wald [2], except that Holz & Wald work in the physical spacetime rather than the conformally transformed spacetime, and at the end of the computation they compute the ratio between the quantity $x_s^2/(\det \mathcal{A})$ evaluated in the perturbed spacetime and in the background spacetime. In our approach we do

not need to compute a ratio, and furthermore the source term in the differential equation (2.14) vanishes in FRW regions between the voids, which simplifies the computation. See Appendix B for more details on the relation between the two approaches.

We now turn to a discussion of the method we use to compute approximate solutions to the differential equation (2.14). Consider a small segment of ray, from $x = x_1$ to $x = x_2$ say. Since the differential equation is linear, we have

$$\begin{bmatrix} \mathcal{A}_B^A(x_2) \\ \dot{\mathcal{A}}_B^A(x_2) \end{bmatrix} = \begin{bmatrix} J_C^A(x_2, x_1) & K_C^A(x_2, x_1) \\ L_C^A(x_2, x_1) & M_C^A(x_2, x_1) \end{bmatrix} \times \begin{bmatrix} \mathcal{A}_B^A(x_1) \\ \dot{\mathcal{A}}_B^A(x_1) \end{bmatrix}. \quad (2.18)$$

for some 2×2 matrices J, K, L, M which together form a 4×4 matrix. To linear order in \mathcal{R}_{AB} we have³

$$J_C^A = \delta_C^A - \int_{x_1}^{x_2} dx (x_2 - x) \mathcal{R}_C^A(x), \quad (2.19a)$$

$$K_C^A = (x_2 - x_1) \delta_C^A - \int_{x_1}^{x_2} dx \int_{x_1}^x d\bar{x} (\bar{x} - x_1) \mathcal{R}_C^A(\bar{x}), \quad (2.19b)$$

$$L_C^A = - \int_{x_1}^{x_2} dx \mathcal{R}_C^A(x), \quad (2.19c)$$

$$M_C^A = \delta_C^A - \int_{x_1}^{x_2} dx (x - x_1) \mathcal{R}_C^A(x). \quad (2.19d)$$

We evaluate these matrices for a transition through a single void, using the potential (2.6), the metric (2.13) and the definition (2.12) of \mathcal{R}_{AB} . We neglect the time evolution of the potential during passage through the void; the corresponding corrections are suppressed by $(H_0 R)^2$. This gives

$$J_C^A = \delta_C^A + c^2 \mathcal{P}(z) \begin{pmatrix} 1 & 4 \\ 4 & 1 \end{pmatrix}, \quad (2.20a)$$

$$K_C^A = (x_2 - x_1) \delta_C^A + \frac{2}{3} c^3 \mathcal{P}(z) \begin{pmatrix} 1 & 2 \\ 2 & 1 \end{pmatrix}, \quad (2.20b)$$

$$L_C^A = 2c \mathcal{P}(z) \begin{pmatrix} 1 - \frac{R^2}{3c^2} & 4 \\ 4 & 1 - \frac{R^2}{3c^2} \end{pmatrix}, \quad (2.20c)$$

$$M_C^A = \delta_C^A + 2c^2 \mathcal{P}(z) \begin{pmatrix} 1 + \frac{R^2}{3c^2} & 2 \\ 2 & 1 + \frac{R^2}{3c^2} \end{pmatrix}. \quad (2.20d)$$

Here b is the impact parameter, $c = \sqrt{R^2 - b^2}$,

$$\mathcal{P}(z) = \frac{3}{2} H_0^2 \Omega_M \frac{x(x_s - x)}{x_s} \frac{f(z)}{a_{\text{ex}}(z)}, \quad (2.21)$$

² In our Monte Carlo simulations we discard all cases where the determinant is negative, and so the absolute value sign in Eq. (2.16) can be dropped. As explained in Ref. [2], this prescription yields the distribution of magnifications of primary images; it is not possible using the geodesic deviation equation method to compute the distribution of total luminosity of all the images of a source.

³ Holz & Wald [2] drop all of the integrals over the projected Riemann tensor in Eqs. (2.19) except the one in the formula for L_C^A . This is valid to leading order in $(H_0 R)^2$. We keep the extra terms in Eqs. (2.19) even though our formalism neglects other effects that also give fractional corrections of order $(H_0 R)^2$. The extra terms change σ_m by a few percent.

and $f(z)$ is defined by Eq. (2.10). In these equations x and z are evaluated at the center of the void.

Our computational procedure can now be summarized as follows:

1. Pick some source redshift z_s , void radius R , and fraction of void mass on the shell today f_0 .
2. Choose void locations according to the prescription described in Sec.II B.
3. For each void, compute the 4×4 matrix that is formed by the matrices $\mathbf{J}, \mathbf{K}, \mathbf{L}$ and \mathbf{M} from Eqs. (2.20).
4. Perform a similarity transformation $\mathbf{J} \rightarrow \mathbf{U}^{-1} \cdot \mathbf{J} \cdot \mathbf{U}$ on each of the matrices $\mathbf{J}, \mathbf{K}, \mathbf{L}, \mathbf{M}$ for some randomly chosen $SO(2)$ matrix \mathbf{U} , to randomize the direction of the vectorial impact parameter.
5. Multiply together all the 4×4 matrices, and multiply by the initial conditions (2.15), to evaluate $\mathcal{A}_B^A(x_s)$.
6. Compute the magnification μ relative to FRW from Eq. (2.16), and then distance modulus shift Δm from

$$\Delta m = -\frac{5}{2} \log_{10}(\mu) \quad (2.22a)$$

$$= \frac{5}{2 \ln 10} \ln |(1 - \kappa)^2 - \gamma^2|. \quad (2.22b)$$

7. Repeat steps 2 to 6 a large number of times to generate the distribution $p(\Delta m; z_s)$ of distance modulus shifts Δm for sources at redshift z_s , for a randomly chosen direction from the observer.
8. Finally, we correct this distribution to obtain the observationally relevant quantity, the probability distribution of magnitude shifts for a source chosen randomly on a sphere at a distance corresponding to redshift z_s . The corrected distribution is [2]

$$\begin{aligned} \mathcal{P}(\Delta m; z_s) &= \mathcal{N} p(\Delta m; z_s) / \mu \\ &= \mathcal{N} p(\Delta m; z_s) 10^{2\Delta m/5}, \end{aligned} \quad (2.23)$$

where \mathcal{N} is a normalization constant.

D. Relation to weak lensing theory

In weak lensing theory the matrix $\mathcal{A}(x_s)/x_s$ that describes the deflections of the rays is presumed to be always very close to the unit matrix, so the total integrated effect of the inhomogeneities on a given ray can be treated linearly. The solution to Eq. (2.14) in this approximation is given by Eq. (2.19b) with $x_1 = 0$, $x_2 = x_s$,

$$\frac{\mathcal{A}_B^A(x_s)}{x_s} = \delta_B^A - \int_0^{x_s} dx \frac{x(x_s - x)}{x_s} \mathcal{R}_B^A(x). \quad (2.24)$$

Taking the determinant and linearizing again, the contribution from shear vanishes and the magnification is $\mu = 1 + 2\kappa$ where the lensing convergence κ is given by the standard formula

$$\kappa = \frac{3}{2} H_0^2 \Omega_M \int_0^{x_s} dx \frac{x(x_s - x)}{x_s a_{\text{ex}}(z)} \delta_m(x). \quad (2.25)$$

Here $\delta_m(x)$ is the fractional over density, x is the comoving distance, x_s is comoving distance to the source, and $a_{\text{ex}}(z)$ is the scale factor. Evaluating this for our void model gives

$$\kappa = \sum_i \kappa_i, \quad (2.26)$$

where the sum is over the voids and

$$\kappa_i = -3H_0^2 \Omega_M \frac{x_i(x_s - x_i)}{x_s a_{\text{ex}}(z_i)} f(z_i) c_i \left[1 - \frac{R^2}{3c_i^2} \right] \quad (2.27)$$

is the lensing convergence from the i th void. Here z_i and x_i are the redshift and comoving distance to the center of the i th void, $c_i = \sqrt{R^2 - b_i^2}$ and b_i is the i th impact parameter. Our model goes beyond the weak lensing result (2.26) as it includes lens-lens couplings and shear.

III. APPROXIMATE ANALYTICAL COMPUTATION OF MAGNIFICATION DISPERSION

A. Overview

In the previous section, we described a Monte Carlo procedure for computing the probability distribution $\mathcal{P}(\Delta m; z_s)$ of magnitude shifts Δm for sources at redshift z_s , for our Swiss cheese model of voids. We will be particularly interested in the mean

$$\langle \Delta m \rangle = \int d\Delta m \Delta m \mathcal{P}(\Delta m; z_s) \quad (3.1)$$

and variance

$$\sigma_m^2 = \int d\Delta m (\Delta m - \langle \Delta m \rangle)^2 \mathcal{P}(\Delta m; z_s) \quad (3.2)$$

of this distribution. In subsequent sections of the paper we will describe the results of our Monte Carlo simulations and their implications. In this section, however, we will take a detour and describe a simple, approximate, analytic computation of the variance. The approximation consists of using the weak lensing approximation to compute the total lensing convergence κ (accurate to a few percent, see Sec. IV B), and then using an approximate cutoff procedure to incorporate the effect of the nonlinear relation (2.22b) between κ and the magnitude shift Δm . We will see in Sec. IV below that this analytic approximation agrees with our Monte Carlo simulations to within $\sim 30\%$.

Neglecting shear, the relation (2.22b) reduces to

$$\Delta m = \frac{5}{\ln 10} \ln |1 - \kappa| \quad (3.3)$$

where κ is given by Eqs. (2.26) and (2.27). We will see shortly that the variance of κ diverges. This divergence is an artifact of our use of a distributional density profile for each void, with a δ -function on the void's surface, and can be removed by endowing each shell with some small finite thickness Δr (see Sec. III D below). The variance of Δm , on the other hand, is finite, because of the nonlinear relation (3.3). We shall proceed by using the linearized version

$$\Delta m = -\frac{5}{\ln 10} [\kappa + O(\kappa^2)] \quad (3.4)$$

of Eq. (3.3), and by simply cutting off the divergent integrals that arise, at $\kappa \sim 1$, the regime where the nonlinearity of the relation (3.3) becomes important.

B. Variance of magnitude shifts

From Eq. (3.4) we find for the mean and variance of the magnitude shift

$$\begin{aligned} \langle \Delta m \rangle &= -\frac{5}{\ln 10} [\langle \kappa \rangle + O(\kappa^2)], \\ \sigma_m^2 &= \left(\frac{5}{\ln 10} \right)^2 [\langle \kappa^2 \rangle - \langle \kappa \rangle^2 + O(\kappa^3)]. \end{aligned} \quad (3.5)$$

The averages are over the set of impact parameters $\{b_i : i \in [1, j(x_s)]\}$ in Eq. (2.27), where $j(x_s)$ is the number of voids out to the source at x_s . In computing the averages, it will prove convenient to define

$$q_i = 1 - b_i^2/R^2, \quad (3.6)$$

so that each q_i is distributed uniformly between zero and one, since impact parameters arbitrarily close to the void boundary are permitted. In fact, a shortcoming of our model is the vanishing thickness of the void wall. We therefore introduce lower cutoffs C_i for each void⁴, that is, we restrict q_i to lie in the range $C_i \leq q_i \leq 1$. We will discuss below the origin and appropriate values of these cutoffs.

With this assumption we obtain for the mean of the lensing convergence (2.27) of the i th void

$$\begin{aligned} \langle \kappa_i \rangle &= -H_0^2 \Omega_M x_s R w_i \int_{C_i}^1 dq_i \left[3\sqrt{q_i} - \frac{1}{\sqrt{q_i}} \right] \\ &= -2H_0^2 \Omega_M x_s R w_i \sqrt{C_i} (1 - C_i) \end{aligned} \quad (3.7)$$

where

$$w_i = \frac{x_i(x_s - x_i)f(z_i)(1 + z_i)}{x_s^2}. \quad (3.8)$$

The mean lensing convergence (3.7) is always negative, since $C_i < 1$; introducing the cutoff leads to a bias toward de-magnification. This is a shortcoming of the model, since for any mass-compensated perturbation $\langle \kappa_i \rangle = 0$ ⁵. Below, we shall ignore small corrections that are powers of C_i , and will take $\langle \kappa_i \rangle = 0$ for all i .

By contrast the second moment $\langle \kappa_i^2 \rangle$ diverges logarithmically in the limit $C_i \rightarrow 0$:

$$\begin{aligned} \langle \kappa_i^2 \rangle &= (H_0^2 \Omega_M x_s R w_i)^2 \int_{C_i}^1 dq_i \left(3\sqrt{q_i} - \frac{1}{\sqrt{q_i}} \right)^2 \quad (3.9a) \\ &= (H_0^2 \Omega_M x_s R w_i)^2 \left[-\ln C_i - \frac{3}{2} + O(C_i) \right] \quad (3.9b) \end{aligned}$$

This divergence is caused by rays that just graze the δ function shell of the void.

Because κ is a sum of κ_i , its mean is the sum of the individual means, but

$$\langle \kappa^2 \rangle = \sum_i \langle \kappa_i^2 \rangle - \sum_{i \neq j} \langle \kappa_i \rangle \langle \kappa_j \rangle \quad (3.10)$$

and therefore

$$\sigma_\kappa^2 = \langle \kappa^2 \rangle - \langle \kappa \rangle^2 = \sum_i (\langle \kappa_i^2 \rangle - \langle \kappa_i \rangle^2). \quad (3.11)$$

Combining this with Eqs. (3.4) and (3.9b) and dropping terms linear in C_i gives for the variance in magnitude shift

$$\sigma_m^2 = \sigma_0^2 \sum_i w_i^2 \left(-\ln C_i - \frac{3}{2} \right), \quad (3.12)$$

where we have defined

$$\sigma_0 = \frac{5H_0^2 \Omega_M x_s R}{\ln 10}. \quad (3.13)$$

We choose the cutoffs C_i to correspond to $\kappa_i \sim 1$, as discussed above; from Eqs. (2.27) and (3.8) this gives

$$C_i = (H_0^2 \Omega_M R x_s w_i)^2. \quad (3.14)$$

The approximate analytic result given by Eqs. (3.8) and (3.12) – (3.14) is plotted in Fig. 10 in Sec. IV B below. It agrees with our Monte Carlo simulations to within $\sim 30\%$, which is reasonable given the crudeness of our analytic cutoff procedure.

⁴ These cutoffs will be used only for construction of our analytical model in this section; they are not used in Monte Carlo simulations in the remainder of the paper.

⁵ To restore this feature we could either scale the contribution from the underdense core downward by a factor of $S_i = 1 + \sqrt{C_i} + C_i$ or scale the contribution from the overdense shell upward by the same factor S_i .

C. Finite sampling effects

In addition to computing the width σ_m^2 of the distribution of magnitude shifts Δm , we now compute a different quantity $\sigma_{m,\text{med}}^2(N)$ which is, roughly speaking, the estimate of the width that one would obtain with N samples Δm_α , $1 \leq \alpha \leq N$, drawn from the distribution. More precisely, this quantity is defined as follows. From the N samples we construct the estimator

$$\hat{\sigma}_m^2 \equiv \frac{1}{N-1} \sum_{\alpha=1}^N \Delta m_\alpha^2 - \frac{1}{N(N-1)} \left(\sum_{\alpha=1}^N \Delta m_\alpha \right)^2. \quad (3.15)$$

This quantity is itself a random variable with expected value $\langle \hat{\sigma}_m^2 \rangle = \sigma_m^2$. However for finite N the median value of the distribution of $\hat{\sigma}_m^2$ can be significantly different from σ_m^2 . We denote this median value by $\sigma_{m,\text{med}}^2(N)$. In the limit $N \rightarrow \infty$ we have $\sigma_{m,\text{med}}^2(N) \rightarrow \sigma_m^2$. We note that realistic supernovae surveys will have no more than $\sim 10^4$ supernovae.

To estimate this median value, we use the fact that for each void i , finite sampling imposes a minimum value on q_i of $q_i \sim 1/N$ on average, which acts like a statistical cutoff in the integral (3.9b). This is in addition to the physical cutoff (3.14) discussed above, which we will denote by $q_{i,c}$ from now on. For N samples $q_{i,\alpha}$, $1 \leq \alpha \leq N$, the probability that all N samples are larger than a value C_i which is larger than $q_{i,c}$ is

$$P_0(< C_i) = \left(\frac{1 - C_i}{1 - q_{i,c}} \right)^N. \quad (3.16)$$

Differentiating once we find that the probability distribution of C_i is

$$P(C_i) = \left| \frac{dP_0(< C_i)}{dC_i} \right| = \frac{N(1 - C_i)^{N-1}}{(1 - q_{i,c})^N}. \quad (3.17)$$

For very large values of N and small $q_{i,c}$ an adequate approximation is

$$P(C_i) \approx N \exp[-N(C_i - q_{i,c})], \quad (3.18)$$

which is properly normalized for $C_i \geq q_{i,c}$ if we extend the range of C_i to infinity, thereby incurring an error $\sim \exp(-N)$.

We now average the expression (3.12) for the width σ_m^2 , using the distribution (3.18) to average over the cutoffs C_i . The result is

$$\begin{aligned} \sigma_{m,\text{med}}^2 &\approx \sigma_0^2 \sum_i w_i^2 \\ &\times \left[\ln N - \frac{3}{2} - \int_0^\infty dx e^{-x} \ln(x + Nq_{i,c}) \right]. \end{aligned} \quad (3.19)$$

If we define

$$\begin{aligned} S(f_0, z_s) &= \sum_i w_i^2, \\ \gamma(Nq_{i,c}) &= - \int_0^\infty dx e^{-x} \ln(x + Nq_{i,c}), \end{aligned} \quad (3.20)$$

then Eq. (3.19) becomes

$$\sigma_{m,\text{med}}^2 \approx \sigma_0^2 \left[S(f_0, z_s) \left(\ln N - \frac{3}{2} \right) + \sum_i w_i^2 \gamma(Nq_{i,c}) \right]. \quad (3.21)$$

The result (3.21) was obtained by averaging over the cutoffs $\{C_i\}$ using the probability distribution (3.18), and is an estimate of the median of the distribution of $\hat{\sigma}_m^2$. Of course the actual value of $\hat{\sigma}_m^2$ computed from a Monte Carlo realization of N lines of sight, or obtained from N observations of magnifications, may differ from the result (3.21). We would like to also estimate the spread in values of $\hat{\sigma}_m^2$. From Eq. (3.12), and taking the variance with respect to the distribution of cutoffs C_i , we find

$$\left(\frac{\Delta \sigma_{m,\text{med}}^2}{\sigma_{m,\text{med}}^2} \right)^2 = \frac{\sum_i w_i^4 \text{Var}(Nq_{i,c})}{\left[\sum_i w_i^2 (\ln C_i + 3/2) \right]^2}, \quad (3.22)$$

where

$$\begin{aligned} \text{Var}(Nq_{i,c}) &= \overline{(\ln C_i)^2} - (\overline{\ln C_i})^2 \\ &= \int_0^\infty dx e^{-x} [\ln(x + Nq_{i,c})]^2 - [\gamma(Nq_{i,c})]^2 \end{aligned} \quad (3.23)$$

Here the overbars denote an expectation value with respect to the probability distribution (3.18). The quantity (3.22) is a measure in the fractional spread in our estimate of the median, and should give a lower bound on the fractional spread in values of $\hat{\sigma}_m^2$.

Two limits of Eqs. (3.21) and (3.22) are especially simple. First, for $Nq_{i,c} \ll 1$, we have $\gamma(Nq_{i,c}) \approx \gamma_E = 0.5772\dots$, the Euler-Mascheroni constant, and also $\text{Var}(Nq_{i,c}) \approx 1.645$ and $-\ln C_i \approx \ln N + \gamma_E$. This gives

$$\sigma_{m,\text{med}}^2 \approx \sigma_0^2 S(f_0, z_s) \left(\ln N - \frac{3}{2} + \gamma_E \right), \quad (3.24a)$$

$$\frac{\Delta \sigma_{m,\text{med}}^2}{\sigma_{m,\text{med}}^2} \approx \sqrt{\frac{1.645}{N_{\text{void}} (\ln N + \gamma_E - 3/2)}}, \quad (3.24b)$$

where $N_{\text{void}} = x_s/(2R)$ is the number of voids and we have used the crude approximation $w_i = \text{constant}$ in the second equation. Second, for $Nq_{i,c} \gg 1$, we have $\gamma(Nq_{i,c}) \approx -\ln Nq_{i,c}$, $\text{Var}(Nq_{i,c}) \approx 1/(Nq_{i,c})^2$, and $\ln C_i \approx \ln q_{i,c}$, and so we obtain

$$\sigma_{m,\text{med}}^2 \approx \sigma_0^2 \left[-\frac{3}{2} S(f_0, z_s) - \sum_i w_i^2 \ln q_{i,c} \right] \quad (3.25a)$$

$$\frac{\Delta \sigma_{m,\text{med}}^2}{\sigma_{m,\text{med}}^2} \propto \frac{1}{N}. \quad (3.25b)$$

The second case (3.25a) coincides with the N -independent width (3.12) – (3.14) computed earlier. We see that the results are dictated by a competition between

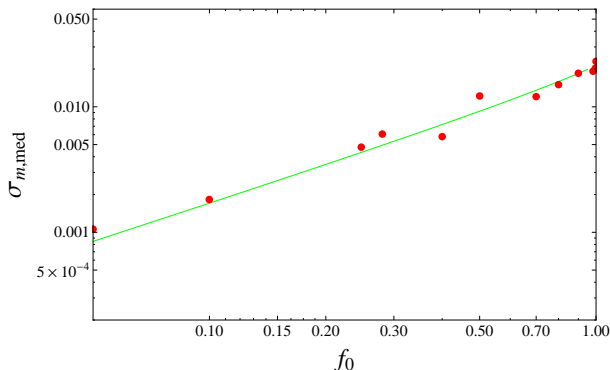


FIG. 1: The green line is our analytic model (3.24a) of the median width of the distribution of magnitude shifts Δm , for $N = 10^4$ samples, source redshift $z_s = 1.0$ and void radius $R = 35$ Mpc, as a function of the fraction of mass f_0 on the void shells today. The data points are from our Monte Carlo simulations with the same parameter values, described in Sec. IV below.

statistical and physical cutoffs via the dimensionless parameter $Nq_{i,c}$.

As discussed above, our simulations are effectively cut off at $\kappa_i \sim 1$; this implies a physical cutoff

$$q_{i,c} \sim (H_0^2 \Omega_M R x_s w_i)^2 \\ \approx 2.2 \times 10^{-7} \left(\frac{H_0 \Omega_M x_s}{0.23} \right)^2 \left(\frac{h_{0.7} R}{35 \text{ Mpc}} \right)^2 (4w_i)^2 \quad (3.26)$$

Here we have scaled the factor $\Omega_M H_0 x_s$ to its value at $\Omega_M = 0.3$, $z_s = 1.0$, the quantity $h_{0.7}$ is given by $H_0 = 70 h_{0.7} \text{ km s}^{-1} \text{ Mpc}^{-1}$, and we note that $4w_i \leq f(z_i)(1 + z_i)$. From the estimate (3.26) we expect the $Nq_{i,c} \ll 1$ limit to apply for $N \lesssim 10^6$. In this case the cutoff is purely statistical and the physical cutoff is unimportant. The prediction (3.24a) for $\sigma_{m,\text{med}}$ for $N = 10^4$ and $z_s = 1$ is shown in Fig. 1, together with results from our Monte Carlo simulations, which are described in Sec. IV below. The plot shows good agreement between the model and the simulations.

For this case, a lower bound on the fractional spread in the values of $\hat{\sigma}_m^2$ around its median value is given by Eq. (3.24b). That is, in any given simulation or observational survey with N light sources, the scatter of values about the expected will be at least this large. For example, with $N = 10^4$, $z_s = 1$ and $R = 35$ Mpc, the implied spread is $\gtrsim 6\%$. In this regime where the cutoff is primarily statistical, the range of likely values of $\hat{\sigma}_m$ is substantial, and only decreases logarithmically with increasing N .

When $N \gtrsim 10^6$, we move into the $Nq_{i,c} \gg 1$ regime where Eqs. (3.25) apply. The results in this regime were discussed in Sec. IIIB above, and are plotted in Fig. 10 in Sec. IVB below. Equation (3.25b) indicates that the spread scales as $1/N$ in this regime. However this estimate is only a lower bound for the spread in values of $\hat{\sigma}_m^2$, as discussed above. In fact, from Eq. (3.15) the standard deviation of $\hat{\sigma}_m^2$ can be computed in terms of N

and of the second and fourth moments of Δm ; it scales like $1/\sqrt{N}$ as $N \rightarrow \infty$. In any case, the spread decreases more rapidly as N increases after the transition to the large N regime. We will see in Sec. IV below that this prediction agrees well with our Monte Carlo simulations.

D. Extension of void model to incorporate finite shell thickness

In this subsection we consider a modification of our void model, in which the void wall is given a finite comoving thickness Δr_i that acts as a physical cutoff in the divergent integral (3.9a). The corresponding value of the cutoff parameter $q_{i,c}$ is $q_{i,c} = 2\Delta r_i/R$, from Eq. (3.6). The value of wall thickness that corresponds to the cutoff (3.26) is thus $\Delta r_i \sim 3 \text{ pc} (R/35 \text{ Mpc})^3$, which is much smaller than the expected void wall thicknesses $\sim \text{Mpc}$ in large scale structure. Thus, our thin-shell void model is somewhat unrealistic; the results are modified (albeit only logarithmically) once the wall thickness exceeds $\sim \text{pc}$ scales. This motivates modifying the model to incorporate a finite wall thickness.

Consider next how the wall thickness evolves with redshift. At very early times, when the perturbation is in the linear regime, it maintains its shape in comoving coordinates, so the cutoff scale is some fixed fraction of R . Once the perturbation becomes nonlinear, the shell thickness should freeze out in physical extent, implying a comoving size $\propto 1/a$. Thus, a suitable model for the redshift dependence of the cutoff would be

$$q_c(a) = \epsilon_0 W(a/a_0), \quad (3.27)$$

where $W(x)$ is a function with $W(x) \rightarrow 1$ for $x \ll 1$ and $W(x) \rightarrow K_0/x$ for $x \gg 1$. Here $a_0(f_0)$ is the scale factor when the perturbation ceases to be linear, and K and ϵ_0 are constants that may also depend on f_0 . Very roughly, we expect $q_c(a) \sim 0.1$ so $Nq_{i,c} \gg 1$ as long as $N \gtrsim 10$, so that Eq. (3.25) will apply.

Suppose now that for a restricted range of source redshifts it suffices to take the fractional shell wall thickness $\epsilon_s = \Delta r_i/R$ in comoving coordinates to be the same for

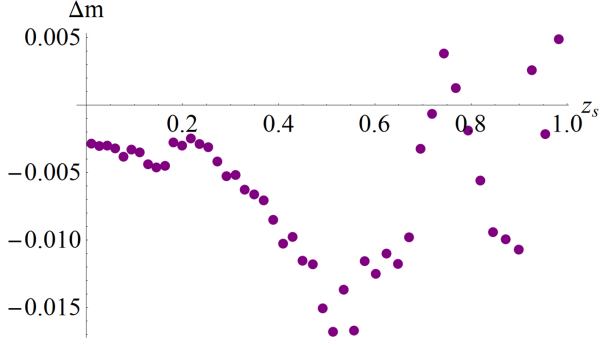


FIG. 2: The magnitude shift Δm as a function of source redshift z_s for a single run, for voids of radius $R = 35$ Mpc, fraction of mass on the shell today $f_0 = 0.9$, in a Λ CDM cosmology with $\Omega_M = 0.3$.

all shells. Then from Eq. (3.12) we get⁶

$$\sigma_m^2 = \sigma_0^2 S(f_0, z_s) [-\ln \epsilon_s + \ln(2) + O(\epsilon_s \ln \epsilon_s)]. \quad (3.29)$$

Equation (3.29) has the same form as Eq. (3.24a), but since $N_{\epsilon_s} \gg 1$, the implied σ_m is smaller. For example, evaluating this expression for $f_0 = 0.9$, $z_s = 1.0$ and $R = 35$ Mpc gives

$$\sigma_m \approx 0.013 \sqrt{1 + 0.23 \ln \left(\frac{1 \text{ Mpc}}{\Delta r} \right)}. \quad (3.30)$$

where $\Delta r = \epsilon_s R$ is the wall thickness.

The logarithmic divergence of σ_m^2 will also be regulated by treating the shell as composed of fragments that represent local density enhancements such as galaxy clusters and superclusters for purposes of computing the magnification of passing light beams. We shall examine this further refinement of our model elsewhere.

IV. RESULTS OF MONTE CARLO SIMULATIONS FOR MAGNIFICATION DISTRIBUTIONS

We now turn to describing the results of our Monte Carlo simulations based on the algorithm described in

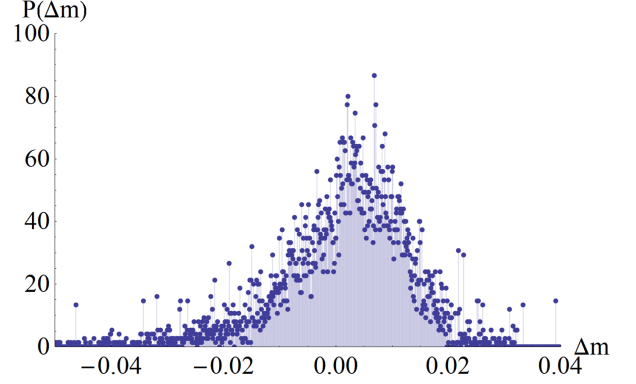


FIG. 3: The probability distribution of magnitude shifts Δm for a simulation in a Λ CDM cosmology with $\Omega_M = 0.3$, with sources at redshift $z_s = 1$, comoving voids radius $R = 35$ Mpc, and fraction of void mass on the shell today $f_0 = 0.9$.

Sec. II. In the remainder of this paper, unless otherwise specified, we will adopt the fiducial parameter values of matter fraction $\Omega_M = 0.3$, source redshift $z_s = 1.0$, void size $R = 35$ Mpc, and fraction of void mass on shell today $f_0 = 0.9$. Our choice of void size is motivated by the fact that observed void sizes [35–43] range from a typical size of ~ 10 Mpc to an upper limit of ~ 100 Mpc. For this fiducial case, we show in Fig. 2 the distance modulus shift Δm as a function of redshift z_s for a single realization of the void distribution. The values jump discontinuously after each void, and illustrate the stochastic nature of the lensing process.

Next, we repeat this computation some large number N of times in order to generate the distribution of modulus shifts Δm . In the rest of the paper we will focus in particular on the mean $\langle \Delta m \rangle$ and standard deviation σ_m of this distribution, and also on the estimator $\hat{\sigma}_m(N)$ of the standard deviation that one obtains at finite N , given by Eq. (3.15), which satisfies $\hat{\sigma}_m(N) \rightarrow \sigma_m$ as $N \rightarrow \infty$.

The distribution for the fiducial case for $N = 2 \times 10^6$ is shown in Fig. 3. For this case the standard deviation is $\sigma_m = 0.03135 \pm 0.0003$ and the mean is $\langle \Delta m \rangle = 0.004 \pm 0.001$ (where the error is estimated based on dividing the data into 200 groups of 10000 runs). Our result for the standard deviation agrees to within $\sim 30\%$ with that of a different Swiss cheese void model by Brouzakis, Tetrakis and Tzavara [29]; see Fig. 5 of that paper which applies to $R = 40$ Mpc voids at $z_s = 1$. It also agrees to within a factor ~ 2 with the predictions of weak lensing theory using an approximate power spectrum for our void model, as discussed in Appendix A.

Figure 4 shows how our estimated standard deviation $\hat{\sigma}_m(N)$ varies with number of runs N . The quantity plotted is $\log_{10} |\hat{\sigma}_m / \sigma_m - 1|$, where $\sigma_m = 0.03135$ is an estimate of the $N \rightarrow \infty$ limit, here taken from our largest run with $N = 10^6$. This plot exhibits several interesting features that are in good agreement with the analytical model described in Sec. III. First, in the low N regime at

⁶ Eq. (3.29) differs from Eq. (3.12) in that the $-3/2$ has been replaced by $\ln 2$. This slightly more accurate version of the equation is derived as follows. Instead of using the cutoff procedure embodied in Eq. (3.9a), we use a regulated density profile of the form $\delta_m(r) = -f\Theta(R_1 - r) + \alpha\Theta(R - r)\Theta(r - R_1)$ where $R_1 = R(1 - \epsilon_s)$ and $\alpha = f[(1 - \epsilon_s)^{-3} - 1]^{-1}$. The variance in the lensing convergence can then be computed from

$$\begin{aligned} \langle \kappa_i^2 \rangle &= 9H_0^4 \Omega_M^2 \frac{x_i^2 (x_s - x_i)^2}{x_s^2 a_{\text{ex}} (x_i)^2 R^2} \int_0^R dr \int_0^R d\bar{r} \delta_m(r) \delta_m(\bar{r}) \\ &\quad \times r \bar{r} \ln \left| \frac{r + \bar{r}}{r - \bar{r}} \right|, \end{aligned} \quad (3.28)$$

from Eq. (2.25).

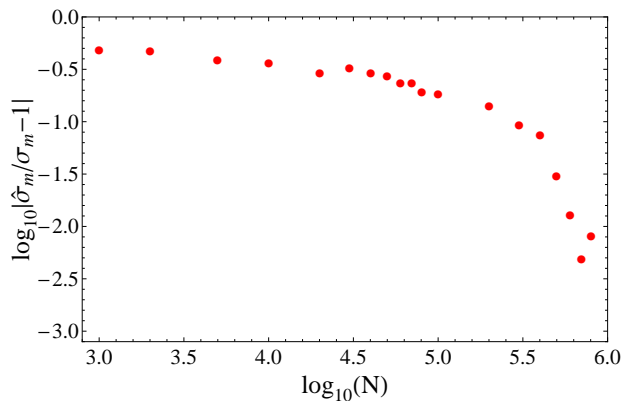


FIG. 4: The estimator $\hat{\sigma}_m$ of the standard deviation of the distribution of magnitude shifts Δm , as a function of number N of runs, for sources at redshift $z_s = 1$, comoving voids radius $R = 35$ Mpc, and fraction of void mass on the shell today $f_0 = 0.9$. The plotted quantity is $\log_{10} |\hat{\sigma}_m / \sigma_m - 1|$, where $\sigma_m = 0.03135$ is an estimate of the $N \rightarrow \infty$ limit, here taken from our largest run with $N = 10^6$.

say $N \sim 10^4$, the values of $\hat{\sigma}_m(N)$ differ systematically from the asymptotic value by a few tens of percent, reflecting the difference between $\sigma_{m,\text{med}}$ and σ_m . Second, there is a somewhat smaller scatter in this regime, of $\sim 5\%$, in agreement with the prediction (3.24b). Third, there is a transition to a different behavior at $N \sim 3 \times 10^5$, after which both the scatter and systematic deviation from the asymptotic value are much smaller.

In the rest of this paper, we will use the value $N = 10^6$ unless otherwise specified. From Fig. 4 this corresponds to an accuracy of ~ 1 percent.

We show in Fig. 5 the mean $\langle \Delta m \rangle$ of the distribution as a function of source redshift z_s , for $R = 35$ Mpc and $N = 2 \times 10^6$. The errors shown are estimated by dividing the data into 200 groups of 10000 runs. The effect of the nonzero mean on cosmological studies cannot be reduced by using a large number of supernovae, unlike the effect of the dispersion σ_m . However, the mean $\langle \Delta m \rangle \sim 0.003$ magnitudes shown in Fig. 5 is too small to impact cosmological studies in the foreseeable future.

In Figs. 6, 7, and 8 we show the probability distributions of magnitude shifts Δm for some other cases: source redshifts of $z_s = 1.1, 1.6$ and 2.1 , and void radii of $R = 35$ Mpc, 100 Mpc, and 350 Mpc. We now turn to a discussion of the dependence of our results on these parameters, as well as on the fraction of mass in the shell today f_0 .

A. Dependence on void size

In Fig. 9 we show the standard deviation σ_m of the magnitude shift as a function of void size R , for three different redshifts, $z_s = 1.1, 1.6, 2.1$. To a good approximation the standard deviation grows as the square root of the void size, $\sigma_m \propto \sqrt{R}$. We can understand this

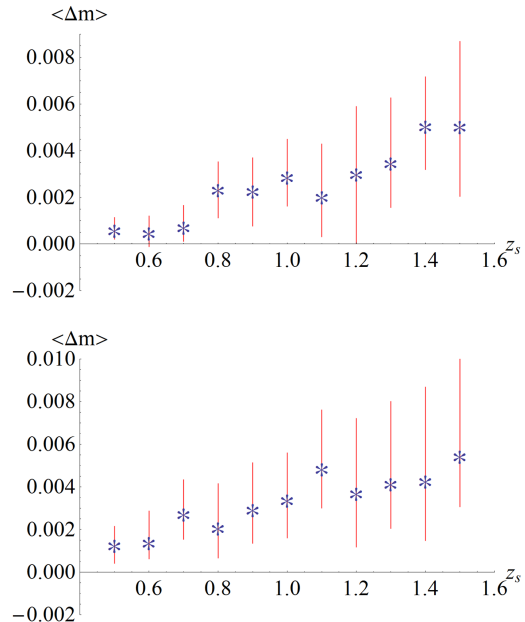


FIG. 5: [Top] The mean $\langle \Delta m \rangle$ of the distribution of magnitude shifts Δm as a function of source redshift z_s , for voids of radius $R = 35$ Mpc with fraction of mass on the shell today $f_0 = 0.9$, for $N = 10^6$ samples. [Bottom] The same for $R = 100$ Mpc.

scaling by making some order of magnitude estimates.

In making these estimates, we consider two different classes of rays. Consider first rays that never come very close to the shell of any of the voids, i.e. we exclude the case $b - R \ll R$, where b is the impact parameter. The potential perturbation $\Delta\phi$ for passage through a void is of order $\Delta\phi \sim f R^2 H_0^2$, where f is the fraction of void mass in the shell (or equivalently the fractional density perturbation in the void interior). The contribution to the lensing convergence from this void is then of order $\kappa \sim \Delta\phi / (H_0 R) \sim f H_0 R$. Next, the trajectory of rays is a random walk, so the net lensing convergence is the rms convergence for a single void multiplied by the square root of the number $\sim 1/(H_0 R)$ of voids. Thus the contribution to the rms magnitude shift from this class of rays is of order

$$\sigma_m \sim f \sqrt{H_0 R}. \quad (4.1)$$

Consider next rays which just graze the shell of at least one of the voids. These grazing rays are subject to large deflections, because of the δ -function in density on the surface of the void. The large deflections cause the second moment $\langle \kappa^2 \rangle$ of the lensing convergence to diverge, as discussed in Sec. IIIB. However, the standard deviation of the magnitude shift Δm is still finite, because of the logarithmic relation (3.3) between Δm and κ .

For estimating the effect of these grazing rays, we neglect shear. The convergence κ of the grazed void will

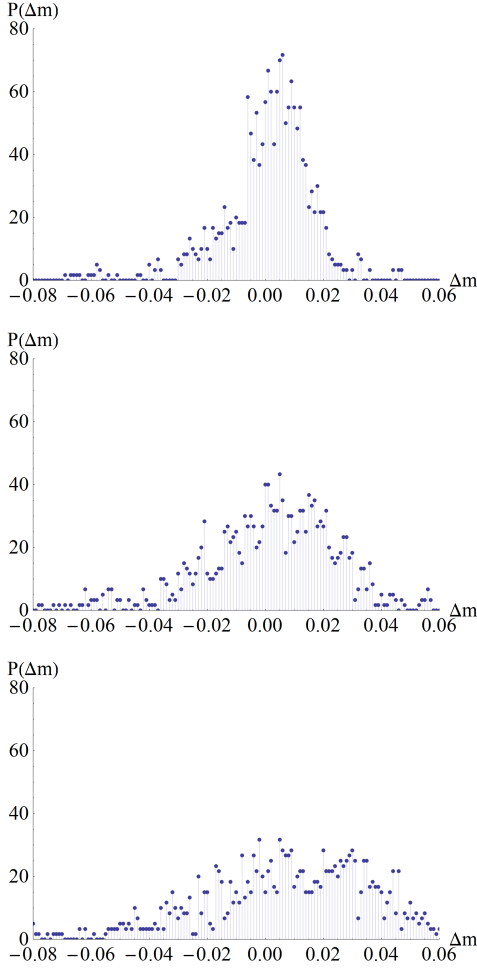


FIG. 6: The probability distributions of magnitude shifts Δm for simulations with sources at redshifts of $z_s = 1.1$ (top), $z_s = 1.6$ (middle) and $z_s = 2.1$ (bottom), for comoving voids of radius $R = 35$ Mpc with 90% of the void mass on the shell today.

be of order unity or larger if the impact parameter b is $b = R(1 - \varepsilon)$, where $\varepsilon \sim f^2 R^2 H_0^2$, from Eq. (2.27). This will occur with probability $\sim \varepsilon$. The contribution of these rays to $\langle (\Delta m)^2 \rangle \propto \langle [\ln(1 - \kappa)]^2 \rangle$ will be of order ε times the number $\sim 1/(H_0 R)$ of voids, or $\sigma_m \sim f\sqrt{H_0 R}$, the same as the result (4.1) for the non-grazing rays.

These considerations show that both the underdense void and the mass-compensating shell make substantial, comparably large contributions to σ_m . This suggests that it may be important to refine the shell model to include its fragmentation into localized overdensities representing galaxy clusters and galaxies, as discussed in Sec. III D above.

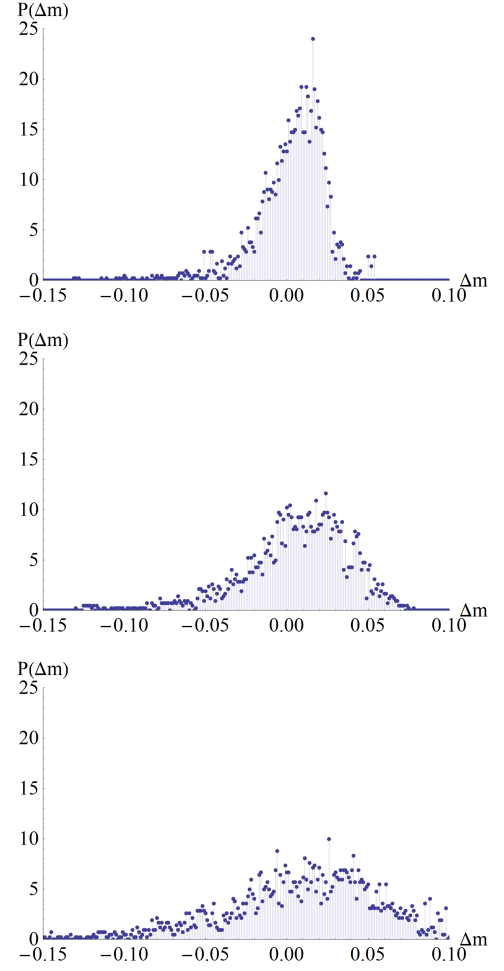


FIG. 7: The probability distributions of magnitude shifts Δm , at source redshifts z_s of 1.1 (top), 1.6 (middle) and 2.1 (bottom), as in Fig. 6 except with comoving void radius of $R = 100$ Mpc.

B. Dependence on fraction of void mass on the shell

In this subsection we discuss the dependence of the magnification distribution on the fraction f_0 of void mass on the shell today, or, equivalently, on the fractional overdensity $\delta\rho/\rho$, cf. Eq. (2.4) above. Figure 10 shows the results of our simulations for σ_m as a function of f_0 for $N = 10^6$, together with a fit of the form (4.2)

$$\sigma_m(f_0) = \alpha f_0 + \beta f_0^2 \quad (4.2)$$

for some constants α and β . We find that $\alpha = 0.025 \pm 0.006$ and $\beta = 0.0085 \pm 0.0064$. Thus, the data show a statistically significant deviation from linear behavior, of the order of $\sim 30 - 40\%$.

We now discuss the various sources of nonlinearity that arise in the computation. We will consider three different types of effects.

First, in weak lensing theory, the magnification is a

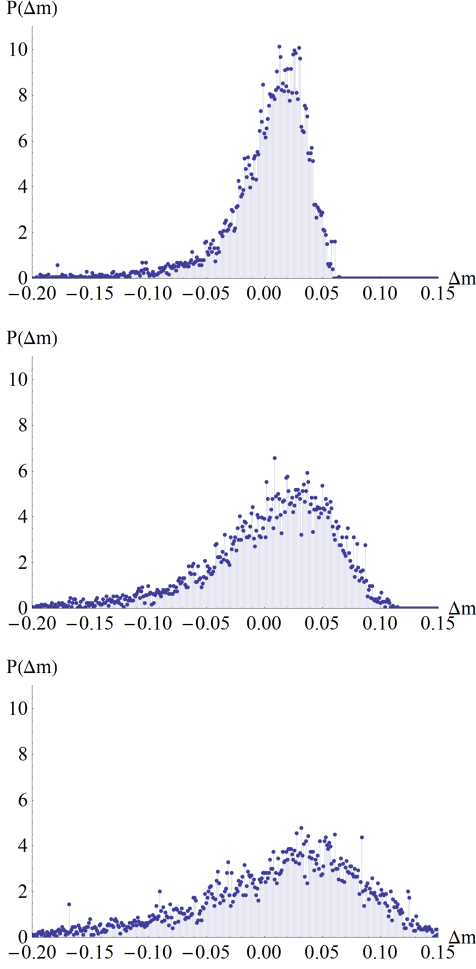


FIG. 8: The probability distributions of magnitude shifts Δm , at source redshifts z_s of 1.1 (top), 1.6 (middle) and 2.1 (bottom), as in Fig. 6 except with comoving void radius of $R = 350$ Mpc.

linear function of the density perturbation. Our computation includes some nonlinear effects that go beyond weak lensing theory, specifically lens-lens coupling (the fact that the deflection due to one lens modifies the deflection caused by subsequent lenses) and shear (the effect of the non-trace components of the matrices \mathcal{R}^A_B and \mathcal{A}^A_B). To explore the magnitude of these effects, we performed Monte Carlo simulations where we compute the lensing convergence for each void and add these to obtain the total lensing convergence (2.26), and then compute Δm from κ using the exact nonlinear relation (2.22b) for zero shear. The resulting value of σ_m for $f_0 = 0.9$, $z_s = 1$, $R = 35$ Mpc, $N = 10^6$ is $\sigma_m = 0.0292$, about 7% smaller than the value $\sigma_m = 0.0314$ obtained by multiplying the 4×4 matrices. Thus, there is a $\sim 7\%$ change from lens-lens coupling and shear. For $R = 100$ Mpc, the change due to lens-lens coupling and shear is $\sim 10\%$. We also performed simulations where we kept just the trace part of the matrix \mathcal{R}_{AB} , in order to exclude the effects

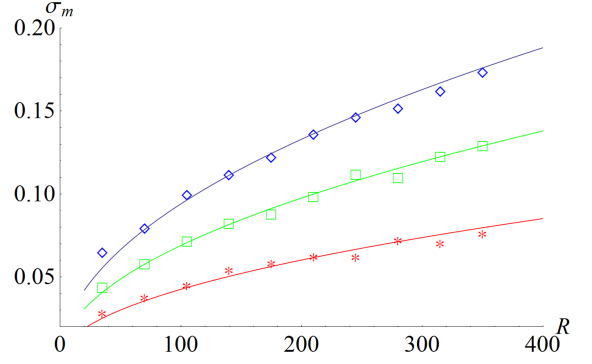


FIG. 9: The standard deviation σ_m of the distribution of distance modulus shifts Δm as a function of void radius R , computed using $N = 10^6$ runs for each point. The bottom line (stars) is for sources at $z_s = 1.1$, the middle line (squares) is $z_s = 1.6$, and the top line (diamonds) is $z_s = 2.1$. Void radii range from 35 to 350 Mpc and the fraction of void mass on the shell today is $f_0 = 0.9$. The lines are fits of the form $\sigma_m \propto \sqrt{R}$.

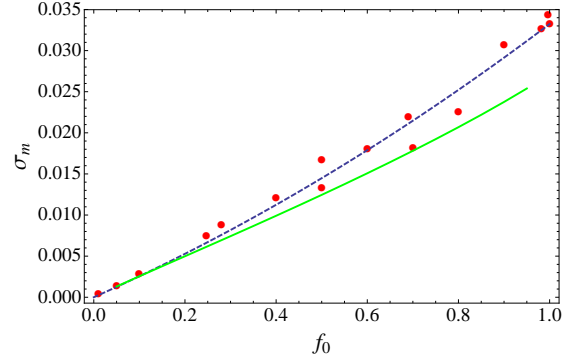


FIG. 10: The standard deviation σ_m as a function of the fraction f_0 of the void mass on the shell today, for void radii of $R = 35$ Mpc and source redshift of $z_s = 1$, computed using $N = 10^6$ runs for each point. The dashed blue curve is a fit of the form $\sigma_m = \alpha f_0 + \beta f_0^2$. This plot shows that there are nonlinearities present at the level of $\sim 30 - 40\%$. The solid green curve is the analytic model (3.12) – (3.14), which is accurate to $\sim 30\%$.

of shear, but included lens-lens couplings by computing 4×4 matrices for each void and multiplying all these matrices. In this case the deviations of σ_m from the full simulations are $\sim 3\%$ for $f_0 = 0.9$, $z_s = 1$, $R = 35$ Mpc and $\sim 6\%$ for $R = 100$ Mpc. Thus, corrections due to shear are of this order.

These nonlinearities due to lens-lens coupling and shear are significantly smaller than the nonlinearity shown in Fig. 10. Thus other sources of nonlinearity must dominate. For the remainder of this subsection we will neglect lens-lens coupling and shear, to simplify the discussion.

A second type of nonlinearity present in our computations is the fact that the void mass fraction $f(z)$ at some

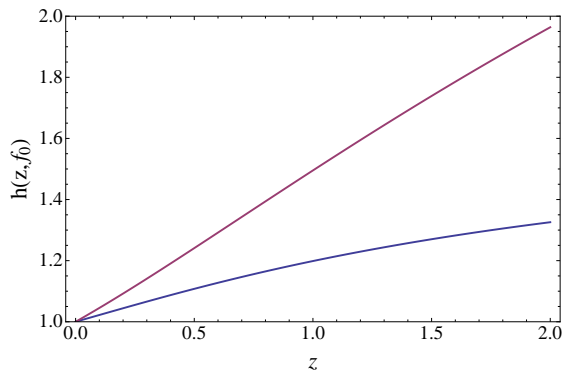


FIG. 11: The factor $h(z, f_0)$ by which nonlinear evolution corrects the growth function $D_+(z)$ of linear perturbation theory, for our void model. The upper curve is for $f_0 = 0.9$ and the lower curve is for $f_0 = 0.5$.

redshift z depends nonlinearly on its value $f_0 = f(0)$ today, due to nonlinearity in the void evolution. Therefore, even if we make the weak-lensing approximation of a linear dependence of the magnification on the density perturbation $f(z)$, the magnification will still be a nonlinear function of f_0 . We can parameterize this nonlinear evolution effect by writing

$$f(z; f_0) = f_0 D_+(z) h(z, f_0), \quad (4.3)$$

where $D_+(z)$ is the growth function of linear perturbation theory, normalized so that $D_+(0) = 1$, and the function $h(z, f_0)$ incorporates the nonlinearity. This function satisfies $h(z, f_0) \rightarrow 1$ as $f_0 \rightarrow 0$ and also as $z \rightarrow 0$, and can be computed using the results of Sec. II A above. Figure 11 plots this function for $f_0 = 0.5$ and $f_0 = 0.9$, and shows that the nonlinearities in the evolution are significant.

This nonlinear evolution effect is the dominant source of nonlinearity in our simulations. To illustrate this, we define, for a given source redshift z_s , the parameter

$$f_{\text{mid}} \equiv f(z_s/2, f_0). \quad (4.4)$$

In other words, f_{mid} is the fraction of void mass on the shell for voids halfway to the source, the distance where most of the lensing occurs. We can use f_{mid} instead of f_0 as a parameter to describe our voids. With this choice of parameterization, the nonlinear evolution effect is significantly reduced. This is illustrated in Fig. 12, which shows the same data as in Fig. 10, but as a function of f_{mid} rather than f_0 . The best fit parameters in the quadratic fit $\sigma_m = \alpha f_{\text{mid}} + \beta f_{\text{mid}}^2$ are now $\alpha = 0.032 \pm 0.005$, $\beta = 0.0016 \pm 0.0057$, showing that there is no statistically significant nonlinearity.

A third type of nonlinearity in our simulations arises from the nonlinear relation between the lensing convergence κ and the magnitude shift Δm . This effect should be present in our data but is quite small. If we neglect lens-lens coupling, shear, and the nonlinear evolution effect, then we expect logarithmic terms in the relation

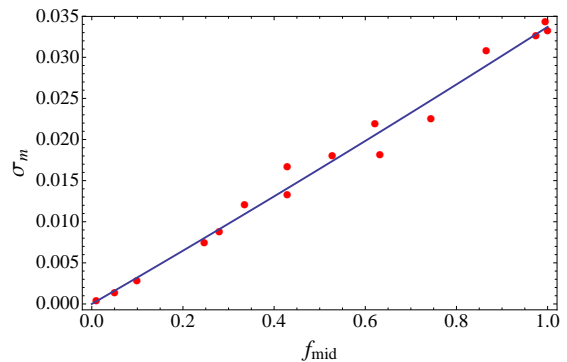


FIG. 12: The standard deviation σ_m as a function of the fraction f_{mid} of the void mass on the shell for voids halfway to the source, for void radii of $R = 35$ Mpc and source redshift of $z_s = 1$. The solid line is a fit of the form $\sigma_m = \alpha f_{\text{mid}} + \beta f_{\text{mid}}^2$. For this choice of parameterization there is no statistically significant nonlinearity detectable in the data.

between σ_m and f_0 , of the form

$$\sigma_m^2 \sim \alpha f_0^2 + \beta f_0^2 \ln f_0 + \dots, \quad (4.5)$$

where α and β are constants which are independent of f_0 . This follows from the analysis of Sec. III B above, where the logarithmic divergence in the variance is cutoff at $\kappa \sim 1$; see Eqs. (3.12) and (3.14). However our data show that the logarithmic terms in Eq. (4.5) are quite small.

Next, we discuss the effects of allowing a distribution of values of void mass fraction on the shell f_0 in our simulations, rather than having a fixed value. We performed simulations where we pick a value of f for each void crossing according to the following prescription. We choose a random values for $1/a_0$ from a Gaussian distribution with a mean of 8 and a variance of 30, truncated to lie in the range that corresponds to $0 \leq f \leq 1$. Figure 13 compares the probability distributions for magnitude shifts with and without variations in f . Treating f as a random variable increases the standard deviation σ_m by $\sim 3\%$.

C. Dependence on source redshift

Figure 14 shows the standard deviation σ_m of the magnitude shift distribution as a function of source redshift z_s , for three different void sizes. The standard deviation increases with redshift faster than z_s . This increase is due in part to the increasing number of voids but there are additional factors.

To understand the redshift dependence analytically we use the expression for the dispersion in lensing convergence from weak lensing theory, given by Eq. (A2) in Appendix A. The matter power spectrum $\Delta(k, z)^2$ for our void model is proportional to $f(z)^2$, so we obtain

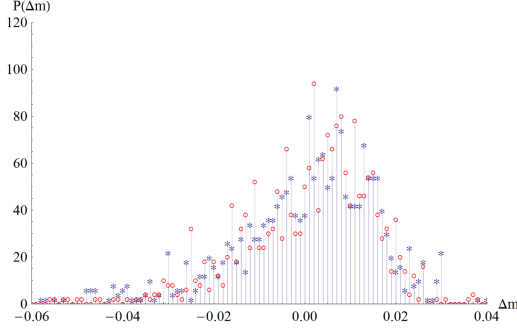


FIG. 13: A comparison of the probability distributions of magnitude shifts Δm in two different cases: fraction of mass on the shell today fixed at $f_0 = 0.9$ (circles), and f_0 drawn from a distribution as described in the text (stars). In both cases void radius is $R = 35$ and source redshift is $z_s = 1.0$. The spread in the shell surface densities gives rise to a wider distribution of magnitude shifts, by about $\sim 3\%$.

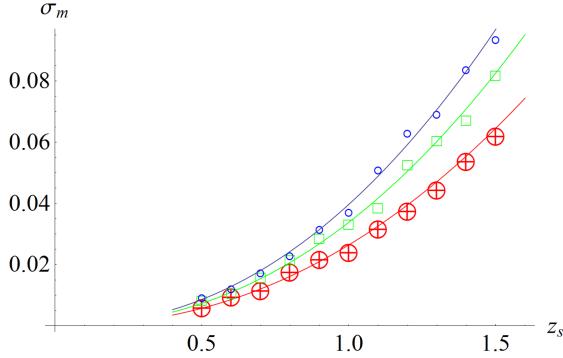


FIG. 14: The standard deviation σ_m as a function of source redshift z_s , computed using $N = 10^6$ runs, for voids of radii $R = 35$ Mpc (red, crossed circles), 70 Mpc (green, squares), and 105 Mpc (blue, circles). The lines are fits proportional to the analytic estimate (4.6).

that

$$\langle \kappa^2 \rangle \propto \int_0^{x_s} dx w(x, x_s)^2 f(z)^2, \quad (4.6)$$

where $w(x, x_s) = (1+z)H_0 x(x_s - x)/x_s$ and $f(z)$ is defined by Eq. (2.10). In the range of redshifts $0.5 \leq z_s \leq 1.5$ this redshift dependence is approximately a power law, proportional to $z_s^{1.35}$, to within $\sim 5\%$ percent⁷. This redshift dependence agrees with the results of our simulations shown in Fig. 14 to within $\sim 10\%$.

⁷ The asymptotic behavior at large z_s is that the expression (4.6) increases linearly in z_s .

D. Numerical fit to parameter dependence

We complete this part of the analysis by giving a three parameter fit for the standard deviation σ_m as a function of void radius R , fraction of void mass on the shell today f_0 , and source redshift z_s . The result is

$$\sigma_m \approx (0.027 \pm 0.0007) \left(\frac{R}{35 \text{ Mpc}} \right)^\alpha \left(\frac{f_0}{0.9} \right)^\beta \left(\frac{z_s}{1.0} \right)^\gamma, \quad (4.7)$$

where the parameters are $\alpha = 0.51 \pm 0.03$, $\beta = 1.07 \pm 0.04$, $\gamma = 1.34 \pm 0.05$. This fit is accurate to $\sim 20\%$ for $35 \text{ Mpc} \leq R \leq 350 \text{ Mpc}$, $0.01 \leq f_0 \leq 0.9$, $0.5 \leq z_s \leq 2.1$.

V. BIAS DUE TO SOURCES OCCURRING PREFERENTIALLY IN HIGH DENSITY REGIONS

For sources which are randomly distributed in space, it is known that the total expected apparent luminosity of a source, including all primary and secondary images, must agree with that of the background FRW model [2]. Hence, in situations where the probability of caustics can be neglected, the probability distribution (2.23) of magnifications μ must be *unbiased*. Biases arise in our computations because of caustic effects, and also because we study the probability distribution of the magnitude shift Δm , which is a nonlinear function of μ , cf. Eq. (2.22a).

However, there is an additional fundamental source of bias which arises from the fact that sources are *not* randomly distributed in space, and instead preferentially occur in high density regions, where they are more likely to be close to a lens. This is the source-lens clustering effect [27]. In this section, we make an analytical estimate of the bias δm of the distribution of magnitude shifts that is due to source-lens clustering in our void model.

In our computations so far in this paper, we have placed the source outside the voids, in the FRW regions. However, in reality most matter is concentrated on the edges of voids, and so sources are more likely to be on the void edges. If we demand that sources always be located on void edges, then the mean of the distribution is shifted by an amount (see derivation below)

$$\delta m = \frac{1}{3 \ln(10)} (1 + z_s) H_0^2 R^2 \Omega_M f_s. \quad (5.1)$$

Here z_s is the redshift of the source and $f_s = f(z_s)$ is the fraction of mass on the shell for voids at the source redshift. Evaluating this estimate for $\Omega_M = 0.3$, $z_s = 1.0$, $R = 35$ Mpc, $f_0 = 0.9$ gives $\delta m \sim 5 \times 10^{-6}$, and $\delta m \sim 5 \times 10^{-4}$ for $R = 350$ Mpc. These biases are below the accuracy of upcoming cosmology surveys.

Turn now to the derivation of the formula (5.1). We start from the standard formula (2.25) for the lensing convergence in weak lensing theory. We consider just the contribution to κ from the last void. In the integral, over

this void, we approximate the factors x and $1/a_{\text{ex}}(z)$ as constants. Writing $\eta = x_s - x$ we obtain

$$\kappa_{\text{last void}} = \frac{3}{2} H_0^2 (1 + z_s) \Omega_M \int_{\text{last void}} \eta \delta_m(\mathbf{x}, t) d\eta. \quad (5.2)$$

We also neglect the time dependence of $\delta_m(\mathbf{x}, t)$ for integrating over the last void.

We now consider two different models for randomizing the relative displacement between the center of the last void and the source. We denote by b the transverse displacement of the void center from the line of sight, as before, and denote by η_v the distance from the void center to the plane through the source perpendicular to the line of sight.

In our first model, we assume b and η_v are randomly distributed, proportional to $b d\eta_v db$, with $0 \leq \eta_v \leq R$ and $0 \leq b \leq R$. Computing the integral (5.2) for our void model (2.4) gives

$$\begin{aligned} \kappa_{\text{last void}} &= \frac{3}{2} H_0^2 \Omega_M (1 + z_s) \\ &\times \begin{cases} -2f_s \eta_v \alpha + \frac{2fR^2 \eta_v}{3\alpha} & \eta_v > \alpha \\ -\frac{1}{2} f (\eta_v + \alpha)^2 + \frac{fR^2}{3\alpha} (\eta_v + \alpha) & \eta_v < \alpha \end{cases} \end{aligned} \quad (5.3)$$

where $\alpha = \sqrt{R^2 - b^2}$. Now averaging over b and η_v gives the expected value of $\langle \kappa_{\text{last void}} \rangle = (1 + z_s) H_0^2 R^2 \Omega_M f_s / 15$.

In the second model, we assume that b and η_v are correlated so that the source is always on the surface of the void. The average of $\kappa_{\text{last void}}(b, \eta_v)$ in this model is

$$\langle \kappa_{\text{last void}} \rangle = \int_0^{\pi/2} \sin \theta \kappa(R \sin \theta, R \cos \theta) d\theta, \quad (5.4)$$

which using the formula (5.3) gives zero. Subtracting the means of the two models gives an estimate of the bias, and multiplying the result by $5/\ln 10$ to convert from $\delta\kappa$ to δm gives the formula (5.1).

VI. CONCLUSIONS

In this paper, we presented a simple model to study the effects of voids on distance modulus shifts due to gravitational lensing. A number of future surveys will gather data on luminosity distances to various different astronomical sources, to use them to constrain properties of the source of cosmic acceleration. The accuracy of the resulting constraints will be degraded somewhat by lensing due to nonlinear large scale structures. We studied this effect by considering a Λ CDM Swiss cheese cosmology with mass compensating, randomly located voids with uniform interiors surrounded by thin shells.

We used an algorithm to compute the probability distributions of distance modulus shifts similar to that of Holz & Wald [2]. The rms magnitude shift due to gravitational lensing of voids is fairly small; the dispersion σ_m

due to 35 Mpc voids for sources at $z_s = 1$ is $\sigma_m = 0.031$, which is $\sim 2 - 3$ times smaller than that due to galaxy clusters (see Appendix A below). Also the mean magnitude shift due to voids is of order $\delta m \sim 0.003 \pm 0.001$. We also studied the bias that arises from the source-lens clustering effect, and estimated that the contribution from voids to this bias is quite small, of order $\delta m \sim 5 \times 10^{-6}$. Refining our model by giving each void shell a finite thickness of ~ 1 Mpc reduces the dispersion σ_m by a factor ~ 2 .

We used our model to estimate the sizes of various non-linear effects that go beyond linear, weak-lensing theory. We estimate that for $R = 35$ Mpc the dispersion σ_m is altered by $\sim 4\%$ by lens-lens coupling, by $\sim 3\%$ by shear. For 100 Mpc voids these numbers become 3% and 6% respectively.

Our simple and easily tunable model for void lensing can be used as a starting point to study more complicated effects. For example, one can use various algorithms to generate realizations of distributions of non-overlapping spheres in three dimensional space. Given such a realization one could use the algorithm of this paper to study correlations between magnifications along rays with small angular separations, which would be relevant to future pencil beam surveys [44]. Finally, our model is complementary to other simplified lensing models in the literature that focus on lensing due to halos but neglect larger scale structures, for example the model of Refs. [18, 19].

Acknowledgments

This research was supported at Cornell by NSF grants PHY-0757735, PHY-0555216, and PHY-0968820 and by NASA grant NNX 08AH27G. RAV acknowledges support from the Kavli Institute for Cosmological Physics at the University of Chicago through grants NSF PHY-0114422 and NSF PHY-0551142 and an endowment from the Kavli Foundation and its founder Fred Kavli.

Appendix A: Comparison with weak lensing theory

In this appendix we show that our results agree moderately well with the predictions of weak lensing theory, by computing an approximate matter power spectrum for our void model. We also obtain an independent estimate of the lensing due to voids by using the power spectrum of the Millennium simulation[15].

It is somewhat complicated to compute an exact power spectrum for our distribution of voids. As a simple model, we choose a two-void probability distribution function for which the locations of the two voids are independently and uniformly distributed inside some large finite volume, except that the probability is set to zero when the distance between the void centers is less than $2R$. For this model, using the void density profile (2.4),

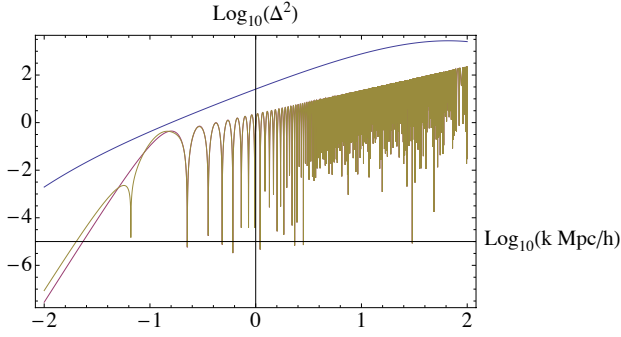


FIG. 15: The estimate (A1) of the matter power spectrum $\Delta(k, z)^2$ for our void distribution, as a function of comoving wavenumber k , evaluated today at $z = 0$. The lower curve includes the correlation correction factor in square brackets in Eq. (A1), and the middle curve omits it. The upper curve is an approximate version of the nonlinear matter power spectrum at $z = 0$ obtained from the Millennium Λ CDM N -body simulation [15], shown for comparison. The parameter values chosen were $H_0 = 73 \text{ km s}^{-1} \text{ Mpc}^{-1}$, $\Omega_M = 0.3$, $f_0 = f(0) = 0.9$, $R = 35 \text{ Mpc}$.

we find for the power spectrum⁸

$$\Delta(k, z)^2 = \frac{2\alpha}{3\pi} f(z)^2 k^3 R^3 j_2(kR)^2 \left[1 - 12\alpha \frac{j_1(2kR)}{kR} \right]. \quad (\text{A1})$$

Here α is the void packing fraction, which is $\pi/6$ in our model, k is wavenumber, j_1 and j_2 are spherical Bessel functions of the first kind, and $f(z)$ is the fraction of the void mass in the shell, which can be computed as a function of redshift using the results of Sec. II A. We note that this power spectrum is not an exact representation of our void model, because in our procedure we first choose a direction to the source and then generate a density perturbation field that depends on this direction. Thus, our procedure does not correspond exactly to choosing a direction randomly in a pre-existing homogeneous, isotropic random process⁹, i.e. $\langle \delta\rho(\mathbf{x})\delta\rho(\mathbf{y}) \rangle$ is not just a function of $|\mathbf{x} - \mathbf{y}|$. Homogeneity is necessary in order to represent the two point function in terms of a power spectrum.

The power spectrum (A1) is shown in Fig. 15, both with and without the correction factor in square brackets that arises from the correlation between void locations. For comparison, we also show in Fig. 15 an esti-

mate of the nonlinear power spectrum¹⁰ obtained from the Millennium simulation [15]. The figure shows that our assumed void model is in rough agreement with the simulation: the two power spectra agree to within a factor $\sim 2-3$ at large scales, for $3 \text{ Mpc} \lesssim k^{-1} \lesssim 30 \text{ Mpc}$, but disagree at small scales $k^{-1} \ll 1 \text{ Mpc}$, where the Millennium spectrum contains more power. This is as expected because our model does not attempt to model structure on these small scales.

We now turn to computing the effects of lensing using these power spectra. From the formula (2.25) for lensing convergence κ in weak lensing theory, it follows that for subhorizon modes the variance in κ is [14, 45]

$$\langle \kappa^2 \rangle = \int d \ln k \left[\frac{9\pi}{4} H_0^2 \Omega_M^2 \int_0^{x_s} dx w(x, x_s)^2 \frac{\Delta(k, z)^2}{k} \right], \quad (\text{A2})$$

where x is comoving coordinate, x_s is the position of the source and $w = (1+z)H_0 x(x_s - x)/x_s$ is the lensing efficiency factor. The corresponding standard deviation in magnitude shift Δm is $\sigma_m = 5\sqrt{\langle \kappa^2 \rangle} / \ln 10$, from Eq. (3.4). We compute the integrand of the $\ln k$ integral by numerically integrating over redshift, for a source redshift of $z_s = 1$. The result is shown in Fig. 16.

Consider first the result for our void distribution. Fig. 16 shows that the envelope of $d\langle \kappa^2 \rangle / d \ln k$ asymptotes to a constant at large k , indicating a logarithmic divergence in the variance $\langle \kappa^2 \rangle$. As discussed in the body of the paper, this divergence is an artifact of our use of distributional density profile for each void, with a δ -function on the void's surface. The divergence can be regulated by endowing each shell with some small finite thickness Δr , which is approximately equivalent to truncating the integral over k in Eq. (A2) at $k \sim 1/\Delta r$. Integrating Eq. (A2) between 10^{-2} Mpc^{-1} and 10^2 Mpc^{-1} gives the result $\sigma_m = 0.011$, which is substantially smaller than the result $\sigma_m = 0.031$ obtained from our nonlinear method in Sec. IV above. The agreement is improved if we integrate up to 10^5 Mpc^{-1} , corresponding the effective cutoff lengthscale in our simulations estimated in Sec. III (even though this shell thickness lengthscale is unrealistic). In this case $\sigma_m = 0.016$, a factor of ~ 2 smaller than our simulations. The factor ~ 2 disagreement is not too surprising, since as mentioned above the derivation of Eq. (A2) requires the assumption that the density perturbation is a homogeneous isotropic random process, which is violated to some extent by our void model.

It is also of interest to compute the standard deviation σ_m for the Millennium simulation spectrum. Figure 16

⁸ This model is not completely consistent, since the power spectrum can become negative for large packing fractions. The inconsistency is presumably a signal that our assumed 2-void probability distribution cannot be obtained starting from any symmetric non-overlapping n -void probability distribution. We ignore this inconsistency here since the correlation effects that give rise to the correction factor in square brackets in Eq. (A1) give only a small ($< 1\%$) correction to $\langle \kappa^2 \rangle$ in any case.

⁹ If the model were exactly homogeneous there would be a nonzero probability for the observer to be located inside a void.

¹⁰ We use the following fit to the Millennium power spectrum, obtained from Fig. 9 of Ref. [15]: $\Delta(k, z)^2 = \alpha(k)(1+z)^{\beta(k)}$, where the functions α and β are chosen so that $\Delta(k)^2 = 1.40889 + 1.67105x - 0.11816x^2 - 0.0356049x^3 - 0.0367596x^4$ at $z = 0$ and $\Delta(k)^2 = 0.87558 + 1.56132x - 0.117482x^2 - 0.0299214x^3 - 0.0383988x^4$ at $z = 0.98$, where $x = \log_{10}(k \text{ Mpc/h})$. This fit is accurate to $\sim 30\%$.

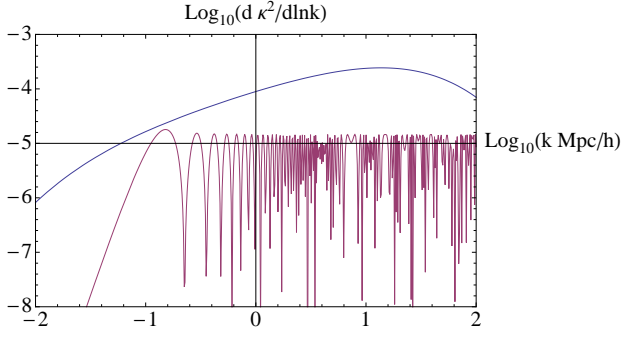


FIG. 16: The variance of the lensing convergence per unit logarithmic wavenumber, $d\langle\kappa^2\rangle/d\ln k$, for a source at redshift $z_s = 1$, computed from the spectra shown in Fig. 15. The upper curve is the Millennium simulation, the lower curve is our void model.

shows that the variance of the lensing convergence per unit logarithmic wavenumber $d\langle\kappa^2\rangle/d\ln k$ peaks at $k \sim 100$ kpc (in agreement with Sec. 10.5 of Ref. [5]). This indicates that lensing is dominated by galactic scale structures, as claimed by Holz & Wald [2]. The total standard deviation¹¹ from all scales $10^{-2}\text{Mpc} \leq k^{-1} \leq 10^3\text{Mpc}$ is $\sigma_m = 0.044$. The standard deviation from integrating only over the scales of voids $3\text{Mpc} \leq k^{-1} \leq 10^3\text{Mpc}$ is $\sigma_m = 0.010$, a factor ~ 4 smaller; this standard deviation agrees well with our estimate (1.2) for the thick-wall void model.

Appendix B: Derivation of procedure for computing magnification distribution

In this appendix we describe in more detail the derivation of our prescription for computing magnifications along a ray given by Eqs. (2.12) – (2.16).

Consider an observer \mathcal{O} and a source \mathcal{S} . The angular diameter distance $D_A(\mathcal{O}, \mathcal{S})$ is defined by

$$D_A^2 = \delta A / \delta \Omega \quad (\text{B1})$$

where δA is the proper area of the source, orthogonal to the direction to the observer, and $\delta \Omega$ is the observed solid angle at the observer subtended by the source. Under a conformal transformation of the metric, $\delta \Omega$ is invariant while δA transforms by a factor of the conformal factor evaluated at the source. It follows that if we define \bar{D}_A to be the angular diameter distance computed in the conformally transformed spacetime (2.13), then we have

$D_A = a(\mathcal{S})\bar{D}_A$, where a is the scale factor. We now define the magnification relative to FRW to be¹²

$$\mu = \frac{D_{A,0}^2}{D_A^2}, \quad (\text{B2})$$

where $D_{A,0}$ is the angular diameter distance computed in the unperturbed FRW model. Expressing the two angular diameter distances in Eq. (B2) in terms of the conformally transformed versions, the factors of $a(\mathcal{S})$ cancel¹³, and we obtain that

$$\mu = \bar{D}_{A,0}^2 / \bar{D}_A^2 = x_s^2 / \bar{D}_A^2, \quad (\text{B3})$$

where x_s is the comoving coordinate of the source.

To compute the angular diameter distance $\bar{D}_A(\mathcal{O}, \mathcal{S})$ in the conformally transformed spacetime (2.13), we use the same method that Holz & Wald [2] used in the physical spacetime, whose derivation we now outline in the context of an arbitrary spacetime. Let $\vec{k} = d/dx$ be the past-directed tangent vector to the null geodesic joining \mathcal{O} and \mathcal{S} , where x is affine parameter with $x = 0$ at \mathcal{O} . We choose vectors $\vec{l}, \vec{e}_1, \vec{e}_2$ at \mathcal{O} so that $\vec{e}_{\hat{\alpha}} = (\vec{k}, \vec{l}, \vec{e}_A)$, $A = 1, 2$ form an orthonormal basis, i.e., satisfy $\vec{k}^2 = \vec{l}^2 = \vec{k} \cdot \vec{e}_A = \vec{l} \cdot \vec{e}_A = 0$, $\vec{k} \cdot \vec{l} = -1$, $\vec{e}_A \cdot \vec{e}_B = \delta_{AB}$. This orthonormal basis is extended along the geodesic by parallel transport.

Now let $\vec{\eta}(x)$ be an infinitesimal connecting vector that joins the geodesic to some nearby geodesic. The components of $\vec{\eta}$ on the orthonormal basis satisfy the geodesic deviation equation $d^2\eta^{\hat{\alpha}}/dx^2 = -R^{\hat{\alpha}\hat{\beta}\hat{\gamma}\hat{\delta}}k_{\hat{\beta}}k_{\hat{\delta}}\eta_{\hat{\gamma}}$. More explicitly, expanding $\vec{\eta} = \mu\vec{k} + \nu\vec{l} + \eta^A\vec{e}_A$, the geodesic deviation equation becomes

$$\ddot{\nu} = 0, \quad (\text{B4a})$$

$$\ddot{\mu} = \nu\mathcal{R} - \eta_C\mathcal{R}^C, \quad (\text{B4b})$$

$$\ddot{\eta}^A = \nu\mathcal{R}^A - \eta_C\mathcal{R}^{AC}. \quad (\text{B4c})$$

Here dots denote derivatives with respect to x , $\mathcal{R} = R_{abcd}k^ak^bk^cl^d$, $\mathcal{R}_A = -R_{abcd}k^ak^bk^ce_A^d$, and $\mathcal{R}_{AB} = R_{abcd}k^ae_A^bk^ce_B^d$.

We are interested in a set \mathcal{B} of rays all of which pass through \mathcal{O} and which define an element of solid angle $\delta\Omega$ at \mathcal{O} . The corresponding deviation vectors $\vec{\eta}(0)$ must vanish at \mathcal{O} , and the initial derivatives $d\vec{\eta}/dx(0)$ are orthogonal both to \vec{k} and to the four velocity of the observer, $\vec{u}_{\mathcal{O}}$. If we specialize the choice of orthonormal basis so that $\vec{u}_{\mathcal{O}} \cdot \vec{e}_A = 0$, then it follows that $\nu = \dot{\nu} = 0$

¹¹ This total standard deviation due to lensing computed using weak lensing theory and the Millennium simulation agrees well with that computed using other methods. For example, the corresponding standard deviation for $z_s = 1.5$ is $\sigma_m = 0.066$, which agrees within $\sim 20\%$ with the standard deviation of the distribution shown in Fig. 1 of Ref. [4].

¹² This definition could equivalently be expressed in terms of luminosity distances D_L , since $D_L = (1+z)^2 D_A$ for any spacetime.

¹³ We neglect the contribution to μ caused by the perturbation in the observed redshift of the source, which enters when we express the magnification in terms of the observed redshift. This effect gives a subdominant contribution to μ for subhorizon modes [46, 47].

at \mathcal{O} , and from Eq. (B4a) we obtain that $\nu(x) = 0$ everywhere. By the linearity of the geodesic deviation equation it now follows that

$$\eta^A(x) = \mathcal{A}_B^A(x) \dot{\eta}^B(0) \quad (\text{B5})$$

for some 2×2 matrix \mathcal{A}_B^A . This matrix satisfies the differential equation (2.14) and initial conditions (2.15) given in Sec. II C above, from Eq. (B4c) with $\nu = 0$. We define the quantity

$$\Delta(\mathcal{O}, \mathcal{S}) = \frac{x_s^2}{\det \mathcal{A}(x_s)}, \quad (\text{B6})$$

which is the so-called van Vleck determinant [48]. One can show that this is invariant under rescaling of affine parameter, under changes of the orthonormal basis that preserve \vec{k} , and under interchange of \mathcal{O} and \mathcal{S} .

We now define a set of angular coordinates $\theta = \theta^A$ that parameterize the solid angle measured by the observer, by $\theta^A = \theta_0^A + \dot{\eta}^A(0)/(\vec{k} \cdot \vec{u}_{\mathcal{O}})$, where θ_0 is the direction to the source. The element of solid angle is then

$$\begin{aligned} \delta\Omega &= \int_{\mathcal{B}} d^2\theta = \frac{1}{(\vec{k} \cdot \vec{u}_{\mathcal{O}})^2} \int_{\mathcal{B}} d^2\dot{\eta}^A(0) \\ &= \frac{1}{(\vec{k} \cdot \vec{u}_{\mathcal{O}})^2 |\det \mathcal{A}(x_s)|} \int_{\mathcal{B}} d^2\eta^A(x_s), \end{aligned} \quad (\text{B7})$$

where we have rewritten the integral using the Jacobian of the transformation (B5).

Now consider the element of area δA measured at the source \mathcal{S} . This is defined to be the area in the rest frame of the source, orthogonal to the direction to the observer. We choose an orthonormal basis $\vec{k}, \vec{l}, \vec{e}_A$ at \mathcal{S} so that the four velocity is $(\vec{k} + \vec{l})/2$, and decompose the connecting vector as $\vec{\eta} = \mu' \vec{k} + \nu' \vec{l} + \eta'^A \vec{e}_A$. Then the area is just $\delta A = \int_{\mathcal{B}} d^2\eta'^A$. Now the two orthonormal bases $(\vec{k}, \vec{l}, \vec{e}_A)$ and $(\vec{k}, \vec{l}, \vec{e}'_A)$ at \mathcal{S} are related by some fixed Lorentz transformation, so we obtain

$$\begin{aligned} \nu &= \nu', \\ \mu &= \mu' + \frac{1}{2} \nu' D^2 + H_{AB} \eta'^A D^B, \\ \eta^B &= H_A^B \eta'^A + \nu' D^B, \end{aligned} \quad (\text{B8})$$

for some $SO(2)$ matrix H_{AB} and vector D^A . Since $\nu = 0$ everywhere it follows that η^A and η'^A are related by an $SO(2)$ transformation, which preserves area, and so $\delta A = \int_{\mathcal{B}} d^2\eta^A(x_s)$. Combining this with Eqs. (B1), (B6) and (B7) now gives for the angular diameter distance

$$D_A(\mathcal{O}, \mathcal{S})^2 = \frac{x_s^2 (\vec{k} \cdot \vec{u}_{\mathcal{O}})^2}{|\Delta(\mathcal{O}, \mathcal{S})|}. \quad (\text{B9})$$

This is independent of the normalization of the affine parameter and of the four-velocity of the source, but does depend on the four-velocity of the observer.

We now apply the formula (B9) to a stationary observer in the perturbed Minkowski spacetime (2.13), to obtain the angular diameter distance \bar{D}_A of Eq. (B3) above. Specializing the affine parameter x to be the comoving coordinate gives $\vec{k} \cdot \vec{u}_{\mathcal{O}} = 1$, and then combining Eqs. (B3), (B6) and (B9) gives the magnification formula (2.16).

Finally, we note that in computing the matrix $\mathcal{A}(x_s)$, we follow Holz & Wald [2] in neglecting the influence of the metric perturbation on the background geodesic, and on the parallel transport of the orthonormal basis. The corresponding corrections to the angular diameter distance have been computed in the weak lensing limit in Refs. [46, 47] and are subdominant for subhorizon modes.

Appendix C: Comparison with other studies of lensing due to voids

Luminosity distance in the context of Swiss Cheese cosmology has been studied by Clifton & Zuntz [28], Brouzakis, Tetrakis & Tzavara [23, 29], Szybka [30] and Biswas & Notari [31]. Other studies in perturbed FRW cosmologies have been done by Holz & Wald [2] and Hui & Greene [49]. In this appendix we summarize the relevant results from this literature and compare with our results.

In Clifton & Zuntz [28], the mean and standard deviation of apparent magnitude shifts are studied for redshifts up to $z_s \sim 1$ in Λ CDM cosmology. One difference between their study and ours is that they model voids using a fully relativistic Lemaitre-Tolman-Bondi model with a smooth choice of density profile, whereas we use a simpler Newtonian model where each void consists of a central uniformly underdense region surrounded by a zero thickness shell. Fractional corrections to the Newtonian approximation scale as $(H_0 R)^2 \sim 0.0001$ for 35 Mpc voids, so a fully relativistic void model is not really necessary; our model is substantially simpler than theirs. A second difference between the two studies is that they choose a configuration of voids where the void centers lie along the line of sight. Due to this choice, the lensing contributions from successive voids add coherently instead of random walking, which significantly changes the magnification probability distribution. Specifically, for $z_s = 1$ and deep voids, Clifton & Zuntz obtain a standard deviation in modulus shift of $\sigma_m \sim 0.01$ (their Fig. 16), similar to our value, but they obtain a mean shift of $\langle \delta m \rangle \sim 0.02$, a factor ~ 10 larger than ours. This difference arises from their lack of randomization of impact parameters.

Other similar studies are those of Brouzakis, Tetrakis & Tzavara [29] and Biswas & Notari [31]. Brouzakis *et al.* also use a fully relativistic Lemaitre-Tolman-Bondi void model with a smooth choice of density profile. They find values of standard deviation σ_m which agree to within $\sim 30\%$ with our model; see their Fig. 5 which applies to $R = 40$ Mpc voids at $z_s = 1$. Brouzakis *et al.* [29] and also Biswas & Notari [31] studied the dependence of

the magnification distribution on void sizes, source redshift, and fractional underdensity in the void interior, and found results which agree qualitatively with ours. The effects of randomizing void impact parameters was also studied by Szybka [30], who found as did we that the dimming effect due to voids is not enough to mimic the effect of dark energy. The effect of shear is also studied by Szybka, who found its effects to be very small, in agreement with our results discussed in Sec. IV B above. The main advantage of our model compared to these studies is simplicity: our model allows us to explore and understand the effects of a wide range of parameter values.

Kainulainen & Marra [18, 19] introduce a different technique to study lensing. While we compute the probability distribution of magnifications by doing Monte Carlo simulations of ray tracing, Kainulainen & Marra [18] develop a method that allows them to rapidly compute an approximate form of the entire probability distribution

through a combination of numerical and analytical techniques. However, their application of this method focus on the lensing due to galaxies and halos, not on the larger-scale structures of sheets and voids, so our study is not directly comparable to theirs. We note however that it should be possible to apply their techniques to compute the lensing due to voids.

Finally, a recent paper by Lavallaz & Fairbairn [50] performs a similar study modeling voids as 30 Mpc Lemaitre-Tolman-Bondi spheres with Kostov parameterization [51]. They assume that the supernovae number density is proportional to the mass density inside voids and they study the redshift range $0.01 < z < 2.0$. They find that if there is essentially no cut off in the lower range of z , the scatter in the inferred equation of state parameter w is about 10%, while imposing a cut off in the lower range of z decreases the scatter.

-
- [1] J. Wambsganss, R. Cen, G. Xu, and J. P. Ostriker, *Astron. J. Lett.* **475**, L81+ (1997).
 - [2] D. E. Holz and R. M. Wald, *Phys. Rev. D* **58**, 063501 (1998).
 - [3] P. Valageas, *Astron. Astrophys.* **354**, 767 (2000).
 - [4] D.E. Holz and E. V. Linder, *Ap.J.* **631** 678 (2005).
 - [5] D. Munshi et al., *Phys. Rep.* **462**, 67 (2008).
 - [6] D. Sarkar, A. Amblard, D. E. Holz, A. Cooray, *Ap. J.* **678**, 1 (2008).
 - [7] D. E. Holz, S. A. Hughes. *ApJ* **629**, 15 (2005).
 - [8] G. Ghirlanda et al. *New J Phys* **8**, 123 (2006).
 - [9] L. Amendola et al., *Phys. Rev. Lett.* **105**, 121302 (2010).
 - [10] C. M. Hirata, D. E. Holz and C. Cutler, *Phys. Rev. D* **124046** (2010); C. Shang, Z. Haiman, *Mon. Not. R. Astron. Soc.* **411**, 9 (2011).
 - [11] A. Cooray, D. E. Holz, D. Huterer, *Ap. J.* **637**, L77 (2006); E. Linder, *JCAP* **0803**, 019 (2008); J. Jonsson et al., *A.&A.* **487**, 467 (2008); A.R. Zentner, S. Bhattacharya, *Astrophys. J.* **693**, 1543 (2009).
 - [12] J. Jonsson, T. Dahlen, A. Goobar, E. Mortsell, A. Reiss, *J. Cosmo. Astropart. Phys.* **6**, 002 (2007).
 - [13] M. Bartelmann, P. Schneider. *Phys Rept* **340**, 291-472 (2001).
 - [14] Y. Wang, D. E. Holz, D. Munshi. *Astrophys J* **572**, L15-L18 (2002).
 - [15] V. Springel, S. D. M. White, A. Jenkins, C. S. Frenk, N. Yoshida, L. Gao, J. Navarro, R. Thacker, D. Croton, J. Helly, J. A. Peacock, S. Cole, P. Thomas, H. Couchman, A. Evrard, J. Colberg, F. Pearce. *Nature* **435**, 629-636 (2005).
 - [16] E. Lawrence et al., *Ap. J.* **713**, 1322 (2010).
 - [17] B. Li et al., *arXiv:1012.1625* (astro-ph).
 - [18] K. Kainulainen and V. Marra, *Phys. Rev. D* **80**, 123020 (2009).
 - [19] K. Kainulainen, V. Marra. *Phys Rev D* **83**, 023009 (2011).
 - [20] R. A. Vanderveld, E. E. Flanagan, I. Wasserman. *Phys Rev D* **78**, 083511 (2008).
 - [21] N. Sugiura, K. Nakao, D. Ida, N. Sakai, and H. Ishihara, *Prog. Theor. Phys.* **103**, 73 (2000).
 - [22] T. Kai, H. Kozaki, K. Nakao, Y. Nambu, and C.-M. Yoo, *Prog. Theor. Phys.* **117**, 229 (2007).
 - [23] N. Brouzakis, N. Tetradis, and E. Tzavara, *JCAP* **0702**, 013 (2007).
 - [24] B. Jain and U. Seljak, *Ap.J.* **484**, 560 (1997).
 - [25] B. Jain et al., *Ap. J.* **530**, 547 (2000).
 - [26] T. Hamana et al., *Ap. J.* **529**, 56 (2000).
 - [27] T. Hamana et al., *Mon. Not. R. Astron. Soc.* **330**, 365 (2002).
 - [28] T. Clifton, J. Zuntz. *Mon. Not. R. Astron. Soc.* **400**, 2185 (2009).
 - [29] N. Brouzakis, N. Tetradis, E. Tzavara, *JCAP* **0804**, 008 (2008).
 - [30] S. J. Szybka. *arXiv:1012.5239v1* [astro-ph.CO].
 - [31] T. Biswas, A. Notari, *JCAP* **0806**, 021 (2008).
 - [32] V. Marra, E.W. Kolb, S. Matarrese, A. Riotto. *Phys Rev D* **76**, 123004 (2007).
 - [33] V. Marra, E. W. Kolb, S. Matarrese. *Phys Rev D* **77**, 023003 (2008).
 - [34] V. Marra. *arXiv:0803.3152v3* [astro-ph] (2008).
 - [35] F. Hoyle, M. S. Vogeley. *ApJ* **607** 751 (2004).
 - [36] H. Mathis, S. D. M. White. *Monthly Notices of the Royal Astronomical Society* **337**, Issue 4, 1193–1206 (2002).
 - [37] S. Gottlber, E. L. Lokas, A. Klypin, Y. Hoffman. *Monthly Notices of the Royal Astronomical Society* **344**, Issue 3, 715–724 (2003).
 - [38] M. Plionis, S. Basilakos. *Monthly Notices of the Royal Astronomical Society* **330**, Issue 2, 399–404 (2002).
 - [39] D. C. Pan, M. S. Vogeley, F. Hoyle, Y.-Y. Choi, C. Park. *arXiv:1103.4156v2* [astro-ph.CO]
 - [40] C. Adami, A. Mazure, M. Pierre, P.G. Sprimont, C. Libbrecht, F. Pacaud, N. Clerc, T. Sadibekova, J. Surdej, B. Altieri, P.A. Duc, G. Galaz, A. Gueguen, L. Guennou, G. Hertling, O. Ilbert, J.P. LeFvre, H. Quintana, I. Valtechanov, J.P. Willis, M. Akiyama, H. Aussel, L. Chiappetti, A. Detal, B. Garilli, V. LeBrun, O. LeFvre, D. Maccagni, J.B. Melin, T.J. Ponman, D. Ricci, L. Tresse. *arXiv:1010.6195v1* [astro-ph.CO]
 - [41] K. Kreckel, E. Platen, M. A. Aragn-Calvo, J. H. van Gorkom, R. van de Weygaert, J. M. van der Hulst, K.

- Kovač, C.-W. Yip, P. J. E. Peebles. arXiv:1008.4616v1 [astro-ph.CO]
- [42] Margaret J. Gellar, J. P. Huchra. *Science* **246**, 4932, 897 - 903, (1989).
 - [43] S. D. M. White, C. S. Frenk, M. Davis, G. Efstathiou. *ApJ* **313**, 505 - 516 (1987).
 - [44] A. Cooray, D. Huterer, D. E. Holz, *Phys. Rev. Lett.* **96**, 1301 (2006).
 - [45] P. Valageas. *A & A* **356**, 771 (2000).
 - [46] C. Bonvin, R. Durrer, M. A. Gasparini, *Phys. Rev. D* **73**, 023523 (2006).
 - [47] E. E. Flanagan, E. Rosenthal, I. Wasserman, *Phys. Rev. D* **79**, 044032 (2009).
 - [48] M. Visser, *Phys. Rev. D* **47**, 2395 (1993).
 - [49] L. Hui, P. B. Greene. *Phys Rev* **D73**, 123526 (2006).
 - [50] A. de Lavallaz, M. Fairbairn, arXiv:1106.1611v1 [astro-ph.CO]
 - [51] V. Kostov, arXiv:0910.2611.